Available online at www.sciencedirect.com
ScienceDirect
Lithos 90 (2006) 223–248
LITHOS
www.elsevier.com/locate/lithos

The S-type Ladybird leucogranite suite of southeastern British Columbia: Geochemical and isotopic evidence for a genetic link with migmatite formation in the North American basement gneisses of the Monashee complex

Alana M. Hinchey *, Sharon D. Carr

Ottawa–Carleton Geoscience Centre, Department of Earth Sciences, Carleton University, Ottawa, Ontario, Canada K1S 5B6

Received 26 June 2005; accepted 10 March 2006
Available online 21 July 2006

Abstract

The 62–52 Ma Ladybird granite (LBG) suite is a peraluminous, leucocratic, S-type, quartz monzonitic to granitic suite which occurs as batholiths, stocks, dikes, sills, and pegmatite veins predominantly in the high-grade rocks of the Shuswap complex, in southeastern British Columbia. The emplacement of the LBG was synchronous with the production of abundant migmatites within Thor–Odin dome of the Monashee complex, an exposure of North American basement, exhumed from depths of ca. 26–33 km by Eocene extensional faults. The LBG and the leucosome in migmatites from Thor–Odin dome have similar major and trace element patterns, and are both characterized by zircons which have inherited Precambrian cores. Whole rock Nd isotope compositions show a range of values for the LBG with $\varepsilon Nd_{(55\ Ma)}$ values from −5.0 to −17.2. The $\varepsilon Nd_{(55\ Ma)}$ for the leucosome samples range from −9.5 to −23.6, overlapping with those of the granitic suite. These data support the interpretation of a genetic link between formation of the LBG suite and melting of North American basement rocks, such as those exposed in the core of Thor–Odin dome. The leucosome samples have lower high field strength element (HFSE) concentrations and positive Eu anomalies, whereas the LBG samples have higher HFSE concentrations and negative Eu anomalies. The similar trace element characteristics suggest that the leucosome from the migmatites and the LBG are related, whereby most of the leucosome samples are cumulates and the LBG samples represent evolved or residual melts. The initial $^{87}Sr/^{86}Sr$ isotope values for both the LBG and leucosome samples have a large range. However, the initial Sr isotopic ratios for the LBG suite are lower than those of the leucosome samples, with $^{87}Sr/^{86}Sr_{(55\ Ma)}$ ranging from 0.70603 to 0.73688 and 0.74256 to 0.76593, respectively. This isotopic discrepancy suggests either: a) isotopic disequilibrium during partial melting in the mid- to lower crust where the leucosome formed, b) the distribution of Sr during partial melting was controlled by different melt-producing reactions, and/or c) isotopic heterogeneity in the source rocks. At least part of the LBG suite likely formed via melting of North American basement rocks that were dominantly of sedimentary origin. Melting of the Proterozoic supracrustal metasedimentary rocks overlying North American basement may also have contributed to the formation of the different phases of the suite found at the regional scale. However, the abundant leucosomes in the basement rocks of Thor–Odin dome may mark the paths along which anatectic melt migrated in the structurally overlying Ladybird granites of the South Fosthall pluton.

Keywords: Leucogranite; Migmatite; Partial melting; Anatexis; Leucosome; Geochemistry

* Corresponding author. Present address: Geological Survey, Department of Natural Resources, Government of Newfoundland and Labrador, P.O. Box 8700, St. John's, NL, Canada A1B 4J6. Tel.: +1 709 729 7725; fax: +1 709 729 4270.
E-mail addresses: alanahinchey@gov.nl.ca (A.M. Hinchey), scarr@ccs.carleton.ca (S.D. Carr).

0024-4937/$ - see front matter © 2006 Elsevier B.V. All rights reserved.
doi:10.1016/j.lithos.2006.03.003

1. Introduction

A relationship between the formation of migmatites and the generation of granites has long been postulated (see Mehnert, 1968; Misch, 1968); although the nature of that relationship is often debated (Sawyer, 1987; Le Breton and Thompson, 1988; Clemens, 1990; Brown and D'Lemos, 1991; Jung et al., 2000; Kalsbeek et al., 2001; Solar and Brown, 2001). Exposures of migmatites and related peraluminous, crustally derived granitic intrusions have provided, in certain instances, evidence of a link between migmatites and granitic plutons (i.e. Barbey et al., 1996; Sawyer, 1998; Kalsbeek et al., 2001; Solar and Brown, 2001; Johannes et al., 2003). This link is further supported by the interpretation that the leucosome portion of most migmatites were derived from partial melts and that migmatites may represent initial stages of crustal anatexis (Ashworth, 1985; Sawyer, 1987; Brown et al., 1995; Barbey et al., 1996; Jung et al., 2000; Kriegsman, 2001).

The relationship between spatially associated, coeval migmatites and granite plutons can be as follows: a) leucosome in migmatites may represent a link between high-grade metamorphism and large-scale granitic intrusions (Brown and D'Lemos, 1991); b) leucosome may have fed, or represent crystal fractionation from, the spatially and temporally related granitic bodies (Kalsbeek et al., 2001; Solar and Brown, 2001; Johannes et al., 2003;); c) leucosome may represent healed pathways that granitic melts followed during emplacement in the crust (Sawyer, 1987; Barbey et al., 1996; Sawyer, 2001); d) migmatites may represent the arrested stage of granite formation (Le Breton and Thompson, 1988; Obata et al., 1994); e) migmatites may represent contact metamorphic effects induced by emplacement of temporally associated plutons (Pattison and Harte, 1988; Jung et al., 2000); or, f) there may be no genetic relationship between migmatite formation and spatially associated granites (White and Chappell, 1990). As there are a variety of possible interpretations of spatially and temporally associated migmatites and plutons, various field and laboratory methods are necessary to evaluate any relationship.

This paper evaluates the potential genetic link between coeval migmatites and Paleocene–Eocene S-type leucogranites in the Omineca Belt of southeastern British Columbia. Precambrian North American basement rocks of the Monashee complex are exposed in structural culminations that were exhumed during early Tertiary extension and tectonic denudation (Fig. 1; Parrish et al., 1988). The Monashee complex consists of high-grade Paleoproterozoic basement rocks and overlying cover rocks which are now largely migmatitic and represent the deepest exposed structural level in the southern Canadian Cordillera. In Thor–Odin dome, of the southern part of the complex, the basement rocks underwent progressive deformation and anatexis. The basement gneiss in the core of the dome underwent anatexis at ca. 56 to 54 Ma based on U–Pb zircon geochronology studies (Vanderhaeghe et al., 1999; Hinchey, 2005; Hinchey et al., in press). The production of leucosome was coincident with emplacement of part of the structurally overlying Ladybird granite suite (LBG) which ranges in age from ca. 62 to 52 Ma (Parrish et al., 1988; Carr, 1992) based on U–Pb zircon geochronology studies. Genetic linkages have been proposed between the melting of basement para- and orthogneiss and the extensive formation of the granitic bodies. Vanderhaeghe et al. (1999) and Hinchey and Carr (2003) have suggested that the melt from which the leucosome in the structurally deeper migmatites was derived may also have been the source of the LBG. The leucosome in the diatexite migmatites of Thor–Odin dome are a suitable source for the LBG because they were a component of a melt (Hinchey et al., in press) which would have enabled large-scale magma transport, their volumetric extent is comparable to that of the plutonic suite, and they have similar compositions as the LBG. These characteristics are associated with diatexite migmatites that are likely to represent source melts of parental granites (Sawyer, 1996).

2. Regional geology

The Canadian Cordillera formed as a result of the Paleozoic to Paleogene accretion of fragments of allochthonous and parautochthonous oceanic sequences, continental slivers, volcanic arcs and sedimentary sequences to the western edge of ancestral North America (Monger, 1989). Mesozoic to Paleogene crustal thickening occurred during convergence between accreted terranes and the North American plate (Fig. 1; Monger et al., 1982; Monger, 1989; Gabrielse and Campbell, 1991). By the Middle Jurassic accreted terranes had begun overriding the pericratonic terranes as well as both the Proterozoic and the Paleozoic to early Mesozoic platformal sedimentary sequences that had accumulated on the paleomargin of North America (Monger et al., 1982). By the mid-Cretaceous, a 50 to 60 km thick crustal welt and a foreland basin had formed, and during the Cretaceous the Rocky Mountain fold and thrust belt (Foreland belt) formed (Price, 1986, and references therein). Crustal thickening and burial of the North American sedimentary sequence and the

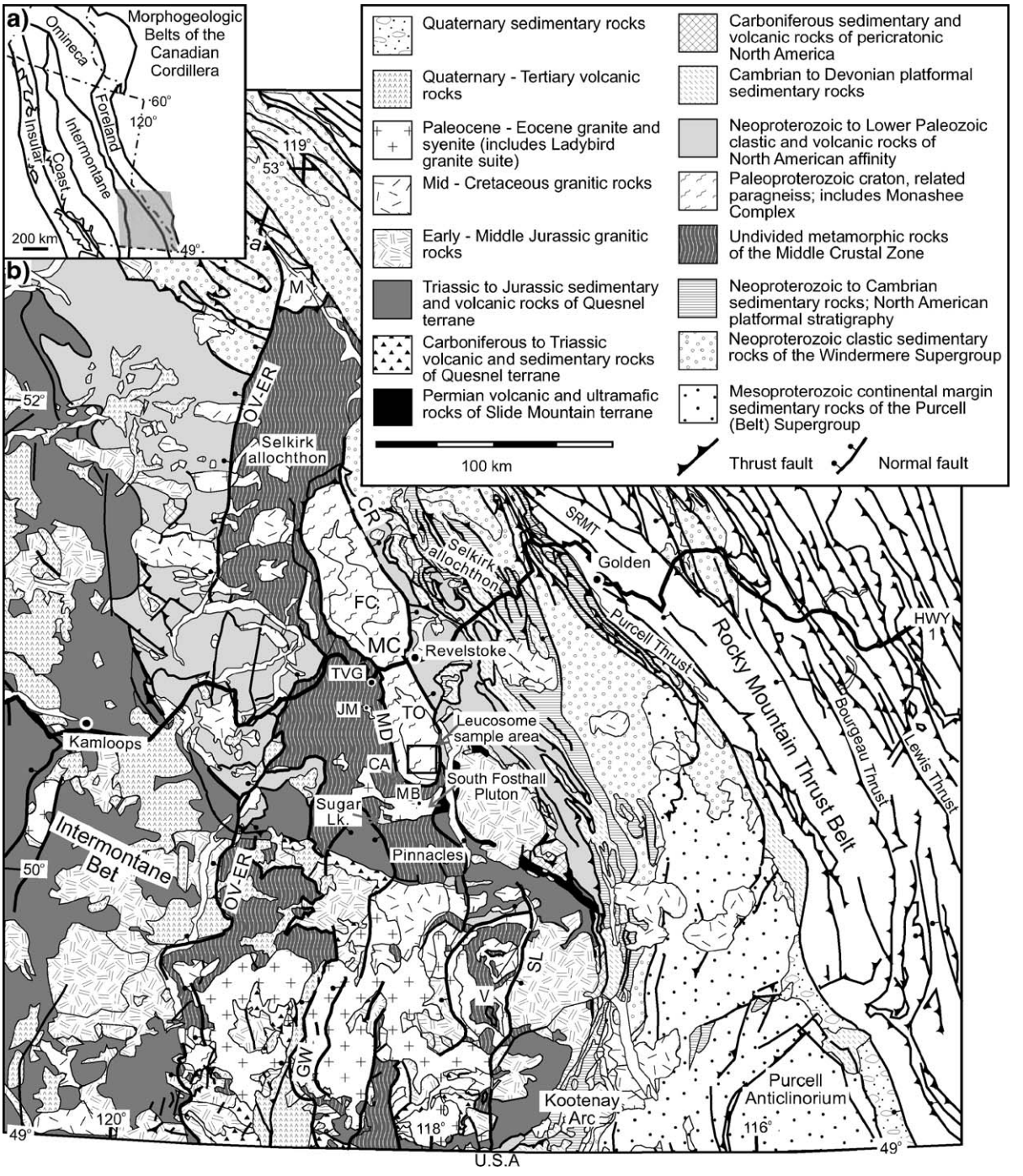

Fig. 1. (a) Map showing the five morphological belts of the Cordillera from Wheeler and McFeely (1991). (b) Tectonic assemblage map of the southeastern Canadian Cordillera (modified after Wheeler and McFeely, 1991). Eocene normal faults include the Okanagan Valley–Eagle River fault system (OV–ER), Columbia River Fault (CR), Greenwood Fault (GW), and Slocan Lake–Champion lake (SL) fault systems. SRMT = Southern Rocky Mountain Trench, M = Malton complex, MD = Monashee décollement, MC = Monashee complex, V = Valhalla complex, FC = Frenchman Cap dome, TO = Thor–Odin dome, TVG = Three Valley Gap, JM = Joss Mountain, MB = Mount Baldur. Sampling areas for the migmatite leucosomes from Thor–Odin and Ladybird granite suite from the South Fosthall Pluton are indicated.

overriding terranes resulted in metamorphism and deformation of rocks in the hinterland of the Rocky Mountain fold and thrust belt, which is termed the Omineca belt. In the Early Tertiary, rocks in what are now southern British Columbia underwent a change from a transpressional to transtensional stress regime (Monger and Price, 2000) that is attributed to changes in the far field stresses related to the obliquity of the downgoing Kula plate (Lonsdale, 1988; Andronicos et al., 2003). This resulted in Eocene regional extension, and the exhumation of some of the high-grade metamorphic rocks of the southern Omineca belt, including the basement rocks of Thor–Odin dome in the southern Monashee complex, via an array of generally north–south striking, brittle and ductile normal faults, which are linked to synchronous strike-slip fault systems that span the western Cordillera (Parrish et al., 1988; Struik, 1993; Johnson and Brown, 1996; Monger and Price, 2000 and references therein).

The southern Omineca belt is characterized by metamorphic and plutonic rocks, structural culminations and belts of high-grade rocks. At the latitude of Thor–Odin dome, high-grade rocks of both the dome and the Middle Crustal Zone, the structurally overlying metasedimentary rocks which dominantly host the LBG (Carr, 1992), have the attributes of a Cordilleran metamorphic complex (Parrish et al., 1988) and are bounded on the eastern and western margins by generally north-striking, outward-dipping Eocene normal faults (Fig. 1; Parrish et al., 1988; Teyssier et al., 2005, and references therein).

In southern British Columbia, periods of arc magmatism occurred during both the Middle Jurassic to late Paleocene transpressional history, when terranes were accreted to the North American continental margin, and during Eocene extensional tectonism (Carr et al., 1987; Armstrong, 1988; Parrish et al., 1988; Carr, 1992). Extensive plutonic activity is divided into four main magmatic episodes: a) Late Triassic to Early Jurassic (215 to 190 Ma); b) Middle to Late Jurassic (180 to 150 Ma); c) Cretaceous (120 to 80 Ma); and d) Early Tertiary (60 to 45 Ma; Armstrong, 1988).

The Early Tertiary magmatic episode included widespread Paleocene to Eocene plutonism that varies in composition and structural style. Within the Shuswap complex, Paleocene to Eocene plutonism is dominated by the LBG (Fig. 1). This 62 to 52 Ma peraluminous leucogranite suite outcrops as synkinematic sheets in both compressional and extensional shear zones, and as late kinematic stocks, plutons and batholiths (Carr, 1992). The bulk of this suite is 55 Ma and occurs between the Okanagan Valley–Eagle River OV–ER fault system and the Slocan Lake fault (SL; Fig. 1). Sevigny et al. (1989) concluded that the 62 Ma peraluminous granites north of the Monashee complex likely formed via partial melting of a pelitic source. As the granites characterized by Sevigny et al. (1989) are geochemically similar and coeval with the LBG, they may represent a northern extension of the suite.

3. Geological setting of the study

The study encompasses the Thor–Odin dome basement rocks and the Middle Crustal Zone rocks in the structurally overlying Thor–Odin Pinnacles area in the southern Omineca belt (Fig. 1). The basement rocks of Thor–Odin dome are composed of heterogeneous migmatitic para- and orthogneisses (Fig. 2). The basement orthogneiss are dominated by migmatitic hornblende–biotite-quartzo feldspathic gneiss with a lesser volume of quartz monzonite gneiss. The basement paragneiss comprise: a) heterogeneous migmatitic garnet–sillimanite-quartzo feldspathic gneiss that are locally enriched in garnet and cordierite considered to be the products of dehydration melting of biotite, b) migmatitic cordierite–biotite-quartzo feldspathic gneiss, and c) minor calc-silicates, marbles, and quartzites (Reesor and Moore, 1971; Duncan, 1984). Though lithologically distinct, the basement ortho- and paragneisses are often interlayered at the scale of a few meters, due in large part to transposition and folding, with contacts that are complicated by the abundance of leucosome. Initial U–Pb geochronology studies of zircons from basement orthogneiss yielded crystallization ages of 1960±45, 1934±6 and 1874±21 Ma (Wanless and Reesor, 1975; Parkinson, 1992). Deposition of part of the basement paragneiss occurred after ca. 2.2 Ga, based on a detrital zircon study of a basement paragneiss and intrusion of ca. 1.9 Ga plutons (Parkinson, 1992). At higher stratigraphic levels deposition of another part of the basement paragneiss occurred after ca. 1.8 Ga, based on the youngest detrital grains obtained from basement paragneiss (Vanderhaeghe et al., 1999; Kuiper, 2003; Hinchey et al., in press). A sequence of supracrustal rocks, interpreted to have been deposited on the basement rocks, is termed the "cover rocks." The cover rocks comprise a heterogeneous assemblage of metasedimentary rocks that includes quartzites, pelitic schists, marbles, calc-silicates, and amphibolites. A preliminary study of the geochronology of detrital zircon in the basal units of the cover gneiss yielded Paleoproterozoic zircons as young as 1825±5 Ma (Kuiper, 2003). There are no constraints on an upper age limit for the cover sequence, and the

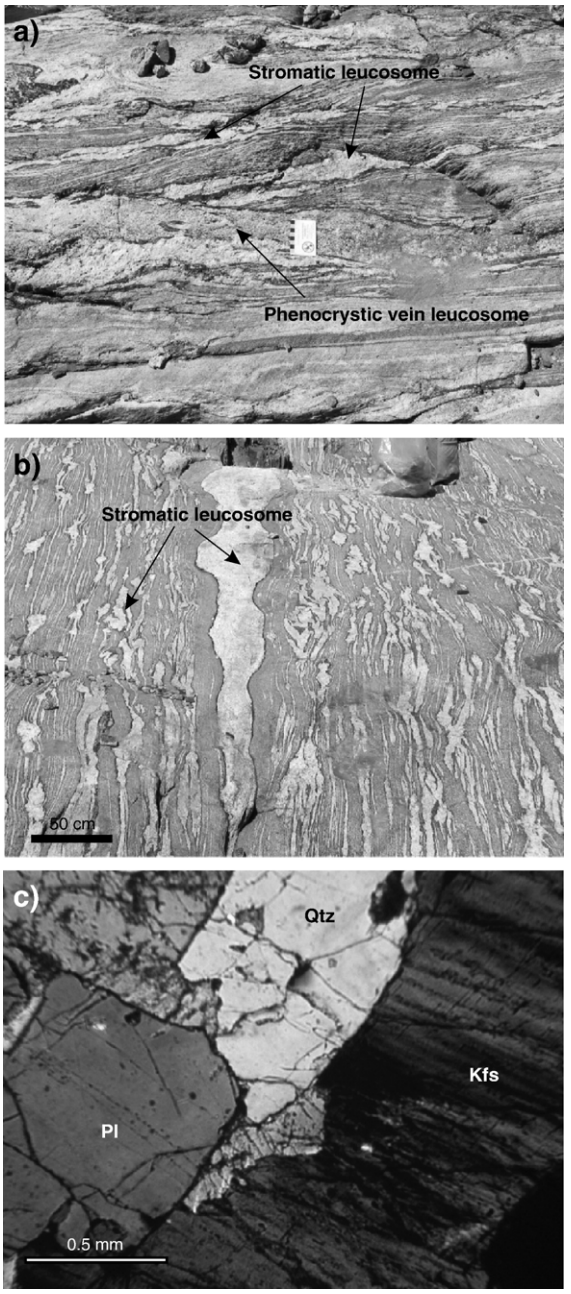

Fig. 2. Representative types of leucosome preserved in migmatitic basement gneisses of Thor–Odin dome. (a) The phenocrystic vein leucosome crosscutting the stromatic leucosome. The host gneiss is the garnet–cordierite–biotite quartzo-feldspathic paragneiss. (b) Host cordierite–biotite–quartz–feldspar paragneiss with folded stromatic type of leucosome. (c) Photomicrograph, in cross-polarized light, of a representative undeformed phenocrystic leucosome sample. Note the euhedral to subhedral grains and lack of alteration in the perthitic orthoclase as evidence of growth in, or from, a melt.

youngest depositional age in Thor–Odin dome is uncertain.

Leucosome occurs pervasively throughout the gneiss of Thor–Odin dome (Fig. 2). Leucosome is interpreted to have formed as a result of in situ melting of the host gneisses (Hinchey, 2005; Hinchey et al., in press). This is based on several lines of evidence summarized from Hinchey et al. (in press), which includes: a) the abundance of leucosome is compositionally controlled, with more melt occurring in semipelitic to pelitic units; b) leucosome is dominantly stromatic leucosome infolded with the basement gneisses, with rare instances of crosscutting vein type of leucosome, indicating contemporaneous folding and anatexis supporting the control of deformation on melt segregation; c) the occurrence of biotite selvages (i.e. melanosome) on the edges of the stromatic leucosome as well as the consistent amount of melanosome relative to leucosome; d) the major and trace element chemistry is consistent with partial melting of the basement paragneiss; d) P–T conditions were 8 to 10 kbar and 800 °C (Norlander et al., 2002) and temperatures were sufficiently high enough to initiate melting of the basement gneisses; e) the area of study preserves the metamorphic assemblage of sillimanite+potassium feldspar+melt, and underwent near isothermal decompression and dehydration melting (see Norlander et al., 2002; Hinchey et al., in press, for melt producing reactions); and g) anatectic zircon has Th/U ratios typical of zircon grown in a partial melting environment.

Leucosome formation in Thor–Odin dome was ongoing from ca. 56 to 54 Ma (Vanderhaeghe et al., 1999; Hinchey et al., in press), coincident with the thermal peak of metamorphism, the formation of at least part of the S_2 transposition foliation, and large-scale F_2 folding (Hinchey et al., in press). Melting may have continued to as young as ca. 51 Ma based on the youngest monazite ages in basement gneiss (Hinchey, 2005). Peak pressures in Thor–Odin dome, on the order of 8 to 10 kbar (Norlander et al., 2002), constrain the depth of burial to between 26 and 33 km. During the anatectic event, the basement paragneiss of Thor–Odin dome were rich in fertile pelites and greywacke layers, providing an obvious source material for the peraluminous, S-type leucogranites that are widespread in the Paleocene–Eocene of the southern Omineca belt.

The LBG suite occurs as dykes, sills, sheets and plutons within the predominantly supracrustal rocks of the Middle Crustal Zone of the Shuswap complex. The peraluminous nature of the granites, presence of inherited Precambrian zircons, lack of occurrence in

the structurally underlying Monashee complex, led to the initial suggestion that the Ladybird granites likely formed via anatectic melting (Carr, 1992). This is supported by general confinement of the LBG suites to the Middle Crustal Zone, which contains abundant sillimanite–potassium feldspar-melt bearing gneiss and schist (Carr, 1992). The South Fosthall pluton is part of the Ladybird granite suite and is the intrusion closest to Thor–Odin dome. The South Fosthall pluton is predominantly composed of sheet-like bodies of pegmatitic leucogranites. Two localities in the South Fosthall pluton yielded U–Pb zircon and monazite ages of 55±1.5 and 55±0.1 Ma (Parrish et al., 1988; Carr, 1992) and inherited Proterozoic zircon cores (Parrish et al., 1988; Carr, 1992; Vanderhaeghe et al., 1999). A third age constraint is from a pegmatite dyke of Ladybird granite near Sugar Lake that has a U–Pb zircon age of 60.5+/−0.5 Ma (Carr, 1992). These ages overlap with the range of ages from the leucosomes of 56 to 54 Ma (Vanderhaeghe et al., 1999; Hinchey et al., in press) from Thor–Odin dome. Due to its proximity to Thor–Odin dome, as well as its known structural setting and age relations, the South Fosthall pluton was chosen as the place to study the link between melting of basement gneisses and granite emplacement. Mapping and sampling was carried out east of Sugar Lake and at Mt. Baldur (South Fosthall creek area; Fig. 1). The boundary of the South Fosthall pluton was originally delineated based on the proportion of pegmatite dykes, greater or less then 50%, relative to screens of metasedimentary rocks by Reesor and Moore (1971). The area has been re-mapped with a new focus on the strain variations in the sheets of Ladybird granite and how this relates to extensional structures by Carr (1990). An isotopic study by Ghosh (1995) of 3 samples of the Ladybird granite suite, from intrusions 120 km south of the South Fosthall pluton, was part of a regional-scale study of the variation in magmatism across the southern Canadian Cordillera. One sample of the LBG was from within the Valhalla complex, and two samples were from the LBG intrusion between the Greenwood Fault and the Okanagan Valley–Eagle River fault system. Ghosh (1995) reported high initial $^{87}Sr/^{86}Sr$ values ranging from 0.706917 to 0.708943, and low εNd values ranging from −6.8 to −13.7, characteristic of granitic melts that have significant crustal contributions.

3.1. Leucosome of the Thor–Odin dome

Leucosomes, defined as the leucocratic part of a migmatite, occur throughout the gneisses of the Thor–Odin dome (Reesor and Moore, 1971; Spark, 2001; McNeill and Williams, 2003). Initial studies suggested that there may be as many as three generations of leucosome production associated with two main melting events; one during the Precambrian and the other during the Cordilleran orogeny (Reesor and Moore, 1971; Spark, 2001; McNeill and Williams, 2003). However, in Thor–Odin dome, U–Pb geochronology studies have constrained leucosome production to a ca. 56 to possibly as young as 52 Ma Cordilleran event (Vanderhaeghe et al., 1999; Hinchey et al., in press). Leucosome is dominantly folded stromatic leucosome, with rare occurrence of younger vein types of: a) phenocrystic vein which are characterized by leucocratic veins containing pheonocrysts of plagioclase and potassium feldspar; and, b) leucocratic pegmatitic vein (Fig. 2a and b). The following description of the leucosome is summarized from Hinchey et al. (in press). Migmatite terminology and definitions are from Ashworth (1985) modified from Mehnert (1968).

The folded stromatic leucosome is the dominant type of leucosome and generally occurs parallel to the foliation and in interconnected veinlets and veins with a well-developed melanosome dominated by biotite (Fig. 2a and b). Melt is interpreted to have formed locally in low strain areas (Hinchey et al., in press). Melt would have mobilized along foliation surfaces, feeding into veinlets and veins (Hinchey et al., in press). The leucosome occurs along the main transposition foliation (S_2), contains a slight foliation defined by the alignment of biotite grains, and is tight to isoclinally folded. The leucosome have a consistent amount of melanosome, are coarse grained, and occur in small veins that tend to pinch and swell along strike, supporting an interpretation of in situ partial melting. Leucosome in crosscutting veins is rare, and descriptions of the two documented types are as follows. The phenocrystic vein type of leucosome is coarse grained, granitic in composition, and has a variable thickness of melanosome dominated by aggregates of coarse biotite crystals. This leucosome is dominated by phenocrysts of potassium feldspar, plagioclase and biotite. This type of leucosome is not folded, does not contain a foliation, and crosscuts the main transposition foliation and the folded stromatic leucosome. The pegmatitic vein type is very coarse grained, granitic in composition and the margins are gradational with foliation parallel leucosome. This leucosome is undeformed, and crosscuts both concordant stromatic and phenocrystic leucosome types, as well as the main transposition foliation.

All leucosome types have similar modal mineralogy, characterized by quartz+potassium feldspar (orthoclase)+plagioclase (An_{12} to An_{33})+biotite± apatite±ilmenite±rutile (Fig. 2c). The quartz, plagioclase, and potassium feldspar primarily occur as euhedral to anhedral grains and often contain abundant inclusions of smaller biotite grains and iron–titanium oxides. Myrmekitic intergrowths of plagioclase and quartz are common, as are primary igneous albite and Carlsbad twinning in plagioclase and potassium feldspar, phenocrysts and cumulate textures. This petrographic evidence supports the conclusion that the leucosome were components of a melt. In situ anatexis is supported by the petrology of the host paragneiss, which contains cordierite, millimeter-scale garnets and minor sillimanite (less than 1%), supporting the involvement of the dehydration reaction of biotite to form garnet, cordierite and melt (Hinchey et al., in press).

3.2. South Fosthall pluton

In the Mt. Baldur area, the LBG intruded as sheets that contain extensive xenoliths of the host gneisses (Fig. 3a). This area is dominated by medium- to coarse-grained, and locally pegmatitic, biotite leucogranite with 20% xenolithic material that is generally 10–20 m thick and as long as 500 m. Some areas are rich in muscovite, tourmaline and garnet; these generally occur near zones of abundant xenoliths. Xenoliths include garnet amphibolite gneiss and heterogeneous biotite quartzo-feldspathic paragneiss with interlayers of quartzite and calc-silicate. Despite the abundance of xenoliths, the LBG at Mt. Baldur is relatively homogenous in composition with only slight variations related to the presence of local mineral phases such as garnet and tourmaline. In the Sugar Lake area, the intrusion is characteristically a medium-grained leucogranite, with few xenoliths (Fig. 3b).

The South Fosthall pluton has a relatively consistent mineralogy. The rocks are dominantly medium- to coarse-grained muscovite–biotite leucogranite. The leucogranites characteristically contain equigranular, euhedral to subhedral, potassium feldspar (orthoclase), quartz, and plagioclase (An_{21} to An_{28}), with accessory biotite and muscovite (Fig. 3c). Potassium feldspar commonly contains biotite inclusions. Primary igneous albite and Carlsbad twins in plagioclase and potassium feldspar are common. Structures such as foliation and lineation in the South Fosthall pluton vary with proximity to extensional shear zones that are

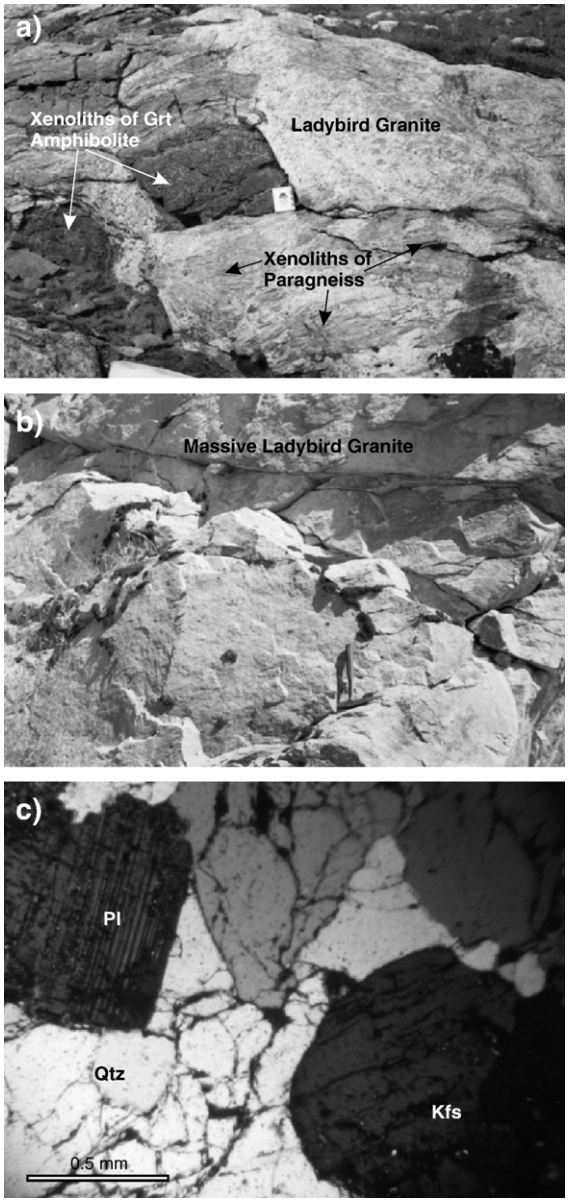

Fig. 3. Representative examples of the Ladybird granite suite. (a) Mt Baldur area, showing that the leucogranite in this region contains xenoliths of garnet amphibolite and paragneiss. (b) Photo is from Sugar Lake and depicts the massive, homogenous nature of leucogranite in this area. (c) Photomicrograph, in cross-polarized light, of a typical Ladybird granite suite sample. Note the euhedral to anhedral grains, lack of alteration of potassium feldspar, and primary albite twinning in plagioclase as evidence of igneous textures.

Eocene or younger in age. Igneous textures such as euhedral grains, cumulate textures, and phenocrysts are preserved in low strain areas. Deformed samples commonly have a preferred orientation of biotite, muscovite, and quartz (the latter exhibits undulose extinction).

4. Analytical data and interpretation

4.1. Major and trace element geochemistry

Major elements, recalculated to an anhydrous total of 100%, and trace element compositions of 13 samples from all styles of leucosome and 16 samples from the Ladybird granite suite were analyzed. Three samples of the Ladybird granite were collected from the Slocan Lake area, in Valhalla complex, for comparison. In addition, six samples of basement gneisses including four samples of basement paragneiss and two samples of basement orthogneiss were analyzed for the purposes of comparison. Sample description and locations are listed in Table 1. Major and trace element data are presented in Table 2. Details of analytical methods are described in Appendix A.1.

4.1.1. Ladybird granite suite

The compositions of the LBG samples define a tight cluster on a Q–A–P diagram with all samples falling in the granite field (Fig. 4). All samples are uniformly felsic and peraluminous on the Shand's index, with K_2O of ~5.5 wt.%, Na_2O of 3.4 wt.% and CaO of <1.1 wt.% (Fig. 5). SiO_2 and Al_2O_3 contents range from 69 to 74 wt.% and from 14 to 16 wt.%, respectively. Na_2O is constant despite increasing SiO_2 levels, while Al_2O_3, Fe_2O_3, CaO, MgO, and TiO_2 tend to decrease slightly with increasing SiO_2 (Fig. 6). The trace element compositions exhibit wide ranges for the low field strength elements, as defined by Saunders et al. (1980), of Ba (221–4032 ppm, mean=1227) and Sr (88–1329 ppm, mean=352; Fig. 7). Most trace element patterns, including those of Sr, Ba and Y, are consistent with major element trends, including those of CaO, MgO and Fe_2O_3, and show a slight decrease in concentration with increasing SiO_2 content. On the basis of major and trace element analyses, there are no chemical distinctions between LBG samples from the South Fosthall pluton and LBG samples from the Valhalla complex; therefore, all samples are treated as one group, although they are plotted using different shaded symbols in Figs. 4 and 8a to illustrate this point.

The chondrite-normalized rare earth element (REE) patterns of the LBG samples are fractionated. Most samples have $La_{(N)}/Yb_{(N)}$ between 80 and 150, whereas six samples have slightly lower ratios with values between 4 and 27, reflecting an enrichment of garnet in some samples (Fig. 8a). The samples have a slight to high negative Eu anomaly, with Eu/Eu* values averaging 0.53 (Table 2). On an extended trace element primitive-mantle normalized variation diagram, the LBG samples exhibit enrichments in elements such as Cs, Rb, Ba, Th, U, Pb and light REEs relative to primitive mantle, and negative Nb–Ta and Ti anomalies (Fig. 8c).

4.1.2. Leucosome from Thor–Odin dome

All but one of the leucosome samples fall within the granite field on a Q–A–P diagram; the one exception falls in the tonalite field (Fig. 4). All of the samples are felsic and peraluminous on the Shand's index (Fig. 5), and show a restricted range in most major element compositions. SiO_2 contents range from 71 to 76 wt.% and Al_2O_3 ranges from 12 to 15 wt.% (Table 2). Na_2O and Al_2O_3 remain constant despite increased SiO_2 levels, whereas Fe_2O_3, CaO, MgO, and TiO_2 tend to decrease with increasing SiO_2 (Fig. 6). The trace element composition of these rocks exhibit large ranges in the low field strength elements of Ba (16–1483 ppm, mean=877) and Sr (14–383 ppm, mean=232; Fig. 7). Trace element variations, such as those of Sr, Ba and Y, are consistent with major element trends, such as those of CaO, MgO and Fe_2O_3, and exhibit a slight decrease in concentration with increasing SiO_2 content.

The chondrite-normalized REE patterns of the leucosome samples are fractionated with $La_{(N)}/Yb_{(N)}$ ranging between 1.5 and 50 times (Fig. 8b). In general, samples with higher SiO_2 concentrations exhibit less fractionation of $La_{(N)}/Yb_{(N)}$. Most leucosome samples show a smooth to strongly positive Eu anomaly with Eu/Eu* values of 0.74 to 5.98; however, two samples show a conspicuous negative Eu anomaly with Eu/Eu* values of 0.15 and 0.22 (Table 2). On an extended trace element primitive-mantle normalized variation diagram, the samples exhibit large enrichments in Cs, Rb, Ba, Th, U, Pb and light REEs relative to primitive mantle, and negative Nb–Ta and Ti anomalies (Fig. 8c).

4.1.3. Comparison of the composition of the Ladybird granite, leucosome, and basement gneiss

The major and trace element compositions of the LBG samples and the leucosomes are similar, in that most samples are peraluminous and granitic in composition. In major element composition, the LBG and leucosome samples are generally indistinguishable and have similar concentrations of most elements (Fig. 6). The leucosome samples show a larger range in certain major elements, including Al_2O_3, CaO, and K_2O. The peraluminous nature is compatible with the LBG being an S-type leucogranite, as classified by Chappell and White (2001); the leucosome samples also fall into this category. In terms of trace element chemistry, the LBG samples tend to have higher concentrations of the high

Table 1
Description and location of the geochemical samples of leucosome, Ladybird granite suite and basement gneisses from the Thor–Odin–Pinnacles area

Sample	Easting	Northing	Sample description	Map location
Ladybird granite samples				
LB-02-01	466,600	5,513,350	Bt leucogranite	Slocan Lake
LB-02-02	466,550	5,513,560	Bt leucogranite	Slocan Lake
LB-02-03	466,700	5,513,220	Bt leucogranite	Slocan Lake
AH-03-03	466,661	5,518,257	Foliated Bt leucogranite	Slocan Lake
AH-03-05	466,410	5,517,365	Foliated Ms–Bt leucogranite	Slocan Lake
AH-03-06	391,283	5,587,489	Foliated Ms–Bt granite	Sugar Lake
AH-03-07	393,055	5,589,929	Bt granite	Sugar Lake
AH-03-13	401,342	5,588,765	Ms–Bt granite	Sugar Lake
AH-03-30	415,498	5,58,6175	Ms Kfs–phenocrystic granite	Mt Baldur
AH-03-31	416,123	5,586,216	Bt granite	Mt Baldur
AH-03-32	416,111	5,586,113	Grt–Ms–Bt granite	Mt Baldur
AH-03-33	415,822	5,585,582	Ms granite	Mt Baldur
AH-03-34	416,348	5,585,952	Ms Kfs–phenocrystic granite	Mt Baldur
AH-03-35	424,173	5,578,737	Foliated Ms–Bt granite	Mt Baldur
AH-03-37	421,983	5,579,663	Bt granite	Mt Baldur
AH-03-38	423,497	5,581,968	Bt granite	Mt Baldur
Leucosome samples				
AH-02-05	423,299	5,600,302	Crosscutting pegmatitic Ms–Bt granitic leucosome	Frigg Glacier
AH-02-06	423,299	5,600,302	Folded stromatic Ms–Bt granitic leucosome	Frigg Glacier
AH-02-08	423,307	5,600,311	Crosscutting pegmatitic Ms–Bt granitic leucosome	Frigg Glacier
AH-02-09	423,239	5,600,301	Stromatic Bt granitic leucosome	Frigg Glacier
AH-02-10	423,270	5,600,336	Folded stromatic Ms–Bt granitic leucosome	Frigg Glacier
AH-02-11	423,291	5,600,689	Folded stromatic Bt granitic leucosome	Frigg Glacier
AH-02-13	423,453	5,600,386	Crosscutting phenocrystic Bt granitic leucosome	Frigg Glacier
AH-02-26	417,252	5,602,040	Sheared, stromatic Bt granititc leucosome	Saturday Glacier
AH-02-27	417,245	5,602,034	Sheared, stromatic Bt granititc leucosome	Saturday Glacier
AH-02-29	417,252	5,602,034	Crosscutting phenocrystic Bt granitic leucosome	Saturday Glacier
AH-03-17	419,010	5,598,756	Crosscutting pegmatitic Ms–Bt granitic leucosome	Bearpaw Lake
AH-03-19	418,966	5,598,825	Phenocrystic Ms–Bt granitic leucosome	Bearpaw Lake
AH-03-22	419,149	5,598,883	Crosscutting pegmatitic Ms–Bt granitic leucosome	Bearpaw Lake
Basement gneisses				
AH-02-07	423,313	5,600,318	Kfs augen granodiorite orthogneiss	Frigg Glacier
AH-02-12	423,299	5,600,669	Bt granodiorite orthogneiss	Frigg Glacier
AH-03-21	419,186	5,598,790	Hbl–Qtz–Kfs–Pl paragneiss	Bearpaw Lake
AH-03-18	419,009	5,598,744	Bt–Qtz–Kfs–Pl paragneiss	Bearpaw Lake
AH-02-28	417,260	5,602,033	Bt Qtz–Kfs paragneiss	Saturday Glacier
AH-02-30	417,243	5,602,028	Grt–Sil–Qtz–Kfs–Pl paragneiss	Saturday Glacier

UTM locations are NAD83 and zone 11.
Mineral symbols are from Kretz (1983).

field strength elements (HFSE) such as Hf, Zr, and Nb, than the leucosome samples (Fig. 7). In addition, the LBG samples generally have higher LREE concentrations and typically display negative Eu anomalies, whereas most of the leucosome samples have positive Eu anomalies. The implications of these characteristics are discussed below. The REE and extended trace element patterns of both the LBG and leucosomes, when compared to average S-type granite composition (data from Chappell and White, 1992; Fig. 8c), show very similar trends and concentrations of elements. The overall geochemical signature of the leucosome and LBG is compatible with granitic melts that are generated via partial melting (dehydration reactions) of the felsic middle to lower crust.

The basement gneisses exhibit a range in major and trace element chemistry, which generally overlaps with that of the LBG and the leucosome samples (Table 2). For most LFSE, the basement samples fall within the field of the LBG and the leucosome samples; however, they commonly show variable concentrations of particular HFSE, such as Nb and Ti, in the gneisses. Differences in the trace element concentrations between

Table 2
Major and trace element chemistry of the leucosome, Ladybird granite suite, and basement gneiss samples from the Thor–Odin–Pinnacles area

	Ladybird granite									
	AH-03-03	AH-03-05	AH-03-06	AH-03-07	AH-03-13	AH-03-30	AH-03-31	AH-03-32	AH-03-33	AH-03-34
(wt.%)										
SiO_2	72.54	74.29	73.85	72.50	74.37	68.95	72.14	72.10	72.81	72.64
TiO_2	0.13	0.11	0.19	0.21	0.13	0.21	0.43	0.04	0.34	0.18
Al_2O_3	14.73	14.22	14.10	14.29	14.61	16.31	14.37	15.90	14.22	14.80
Fe_2O_3*	0.51	0.51	0.67	0.64	0.67	0.82	1.19	0.79	0.94	0.58
FeO	0.55	0.55	0.74	0.65	0.76	0.72	1.46	0.89	1.08	0.58
MnO	0.02	0.02	0.02	0.02	0.02	0.01	0.02	0.07	0.02	0.01
MgO	0.21	0.25	0.24	0.30	0.21	0.43	0.58	0.24	0.46	0.34
CaO	1.52	1.01	0.87	0.92	0.90	0.69	1.27	1.37	0.97	0.83
Na_2O	3.48	3.33	3.46	3.50	3.56	2.68	3.29	3.55	2.88	3.10
K_2O	5.56	5.60	5.27	6.14	4.89	8.48	4.61	5.19	5.65	6.71
P_2O_5	0.21	0.07	0.06	0.13	0.13	0.10	0.08	0.08	0.06	0.08
Sum	99.45	99.96	99.47	99.30	100.24	99.40	99.44	100.21	99.43	99.84
(ppm)										
V	9	11	7	9	9	16	17	6	15	6
Cr	149	176	190	170	165	1	3	5	146	6
Co	5	5	<LD	4	3	2	7	3	10	2
Ni	12.0	<LD	<LD	<LD	183	<LD	<LD	56	<LD	<LD
Zn	24	16	40	31	47	24	52	10	39	14
Ga	24	19	22	27	29	18	17	14	16	17
As	<LD	<LD	<LD	<LD	<LD	<LD	<LD	<LD	<LD	<LD
Rb	232.0	218.0	203.0	252.0	224.0	223.0	170.0	138.4	164.0	225.0
Sr	327.1	239.1	240.1	247.2	88.3	322.9	397.1	189.2	383.8	162.3
Y	14.1	18.8	9.3	6.0	17.9	16.4	7.2	20.7	6.0	4.9
Zr	42.4	59.6	107.3	85.1	71.0	40.4	171.7	50.9	134.7	14.9
Nb	36.0	31.6	14.0	8.3	19.5	7.4	11.6	1.4	11.1	7.5
Cs	8.8	2.9	2.8	4.4	1.9	2.5	1.8	1.5	1.2	3.3
Ba	687	613	818	738	221	1706	3436	688	4032	711
La	20.9	53.9	66.7	47.9	27.7	107.0	88.0	28.1	79.0	27.0
Ce	39.3	105.8	125.2	88.6	56.7	275.0	172.0	58.6	172.0	54.4
Pr	4.3	11.8	13.5	9.3	6.5	27.0	21.3	6.7	19.7	6.1
Nd	14.7	40.9	45.8	31.5	22.9	118.0	71.0	24.3	65.9	21.5
Sm	3.03	8.34	8.66	5.40	5.87	20.20	8.93	5.00	8.48	4.37
Eu	0.71	0.99	0.73	0.81	0.33	1.73	1.60	1.18	1.68	1.01
Gd	2.60	6.38	6.02	3.21	5.03	13.28	4.82	3.86	4.70	3.20
Tb	0.44	0.88	0.69	0.35	0.75	1.43	0.49	0.56	0.46	0.37
Dy	2.56	4.22	2.74	1.45	3.79	5.36	1.88	3.43	1.69	1.51
Ho	0.45	0.70	0.37	0.23	0.65	0.67	0.28	0.78	0.23	0.19
Er	1.14	1.72	0.76	0.52	1.63	1.14	0.63	2.94	0.50	0.35
Tm	0.14	0.23	0.08	0.07	0.22	0.10	0.08	0.60	0.06	0.03
Yb	0.79	1.39	0.48	0.43	1.28	0.52	0.52	5.08	0.41	0.17
Lu	0.10	0.19	0.06	0.06	0.18	0.04	0.07	0.84	0.06	0.02
Hf	1.50	2.10	3.60	2.60	2.60	1.30	3.80	1.80	3.10	0.50
Ta	4.82	2.12	0.65	0.50	0.67	0.50	0.33	0.41	0.32	0.30
Pb	42	59	50	36	39	74	29	46	34	54
Th	9.02	31.30	39.29	21.68	15.59	62.13	28.82	10.67	27.56	11.53
U	13.43	8.32	15.62	4.14	5.89	4.93	2.59	2.72	1.92	1.84
Eu/Eu*	0.77	0.41	0.31	0.59	0.19	0.32	0.75	0.82	0.81	0.83

	Ladybird granite							Leucosome		
	AH-03-35	AH-03-37	AH-03-38	LB-02-01	LB-02-02	LB-02-03	Mean	SEM[a]	AH-02-05	AH-02-06
(wt.%)										
SiO_2	73.55	71.15	73.04	72.50	72.46	72.70	72.60	0.81	71.56	72.16
TiO_2	0.21	0.13	0.17	0.24	0.17	0.12	0.19	0.06	0.39	0.10

Table 2 (*continued*)

	Ladybird granite							Leucosome		
	AH-03-35	AH-03-37	AH-03-38	LB-02-01	LB-02-02	LB-02-03	Mean	SEM[a]	AH-02-05	AH-02-06
Al_2O_3	14.37	15.89	14.66	14.01	13.91	14.23	14.66	0.54	14.10	14.67
Fe_2O_3*	0.77	0.71	0.76	0.71	0.59	0.49	0.71	0.13	0.98	0.47
FeO	0.87	0.70	0.79	0.82	0.67	0.56	0.77	0.16	1.55	0.58
MnO	0.01	0.04	0.07	0.02	0.01	0.01	0.02	0.01	0.03	0.02
MgO	0.26	0.24	0.26	0.33	0.30	0.33	0.31	0.08	0.83	0.27
CaO	1.01	1.14	1.08	1.33	0.97	1.23	1.07	0.18	2.73	2.06
Na_2O	3.43	3.90	3.42	3.15	3.31	3.62	3.35	0.22	4.41	3.70
K_2O	5.23	6.03	6.08	5.29	5.31	4.89	5.68	0.63	1.28	4.27
P_2O_5	0.11	0.04	0.07	0.06	0.07	0.06	0.09	0.03	0.04	0.04
Sum	99.83	99.97	100.39	98.46	97.77	98.25			97.91	98.33
(ppm)										
V	5	17	7	15	14	4	10	4	30	15
Cr	161	155	172	2	4	5	94	79	29	7
Co	1	4	<LD	5	2	5	4	2	11	5
Ni	52	<LD	<LD	8	23	30	52	39	33	67
Zn	31	24	22	44	22	33	30	10	37	19
Ga	25	21	21	22	18	22	21	3	18	18
As	<LD	<LD	<LD	<LD	2	2			1	1
Rb	255.0	135.8	208.0	196.3	209.7	187.1	202.6	28.0	92.1	150.9
Sr	177.9	1329.0	146.1	513.0	438.1	442.7	352.7	173.4	245.9	307.0
Y	8.5	8.3	14.1	8.2	9.6	8.7	11.2	4.4	6.2	10.7
Zr	92.3	140.6	63.8	141.2	116.3	107.1	90.0	36.4	84.8	64.1
Nb	11.6	13.1	14.9	17.4	26.1	16.3	15.5	6.7	14.9	5.0
Cs	3.5	1.2	2.8	2.6	3.4	2.1	2.9	1.1	3.2	1.9
Ba	590	1651	331	1320	1012	1084	1227	751	184	968
La	67.2	11.0	38.0	79.4	65.4	70.6	54.9	23.0	9.7	26.2
Ce	136.0	20.9	87.5	136.7	114.5	121.7	110.3	46.3	18.1	48.6
Pr	13.9	2.2	9.8	17.5	14.3	15.3	12.4	5.4	2.0	5.8
Nd	46.8	7.9	34.3	55.2	44.7	47.5	43.3	18.6	6.6	19.0
Sm	8.11	1.49	7.51	9.13	7.81	8.10	7.53	2.50	1.31	3.80
Eu	0.73	0.51	0.47	1.83	1.35	1.40	1.07	0.41	0.62	1.27
Gd	4.84	1.29	5.34	5.80	5.20	5.43	5.06	1.50	1.23	3.15
Tb	0.53	0.21	0.64	0.68	0.65	0.69	0.61	0.19	0.20	0.48
Dy	2.19	1.35	2.92	2.24	2.30	2.35	2.62	0.84	1.07	2.13
Ho	0.32	0.29	0.56	0.30	0.33	0.33	0.42	0.16	0.22	0.42
Er	0.72	0.89	1.94	0.57	0.69	0.56	1.04	0.53	0.57	0.99
Tm	0.09	0.14	0.38	0.07	0.10	0.07	0.15	0.10	0.09	0.15
Yb	0.55	0.96	3.16	0.45	0.59	0.39	1.07	0.83	0.50	0.84
Lu	0.08	0.14	0.58	0.06	0.09	0.06	0.16	0.14	0.09	0.13
Hf	2.90	3.90	2.30	4.19	3.56	3.30	2.69	0.85	2.36	2.97
Ta	0.49	0.90	0.96	0.66	1.72	0.48	0.99	0.71	1.09	0.39
Pb	45	9	46	39	40	38	43	10	13	32
Th	28.93	6.37	25.79	36.07	30.28	34.35	26.21	10.35	5.31	16.21
U	5.91	1.92	7.30	5.63	7.25	5.67	5.94	2.78	2.97	5.34
Eu/Eu*	0.35	1.12	0.23	0.77	0.65	0.65			1.49	1.12

	Leucosome									
	AH-02-08	AH-02-09	AH-02-10	AH-02-11	AH-02-13	AH-02-26	AH-02-27	AH-02-29	AH-03-17	AH-03-19
(wt.%)										
SiO_2	74.38	71.88	75.02	73.20	72.73	70.29	74.37	74.07	75.84	73.48
TiO_2	0.05	0.24	0.06	0.03	0.21	0.17	0.40	0.03	0.09	0.03
Al_2O_3	13.60	14.01	13.49	14.17	13.72	14.91	12.00	14.00	14.28	14.78
Fe_2O_3*	0.33	0.95	0.18	0.16	0.75	0.57	1.16	0.25	0.51	0.36

(continued on next page)

Table 2 (*continued*)

	Leucosome									
	AH-02-08	AH-02-09	AH-02-10	AH-02-11	AH-02-13	AH-02-26	AH-02-27	AH-02-29	AH-03-17	AH-03-19
FeO	0.42	1.21	0.21	0.18	0.90	0.57	1.77	0.29	0.63	0.34
MnO	0.02	0.03	0.01	0.01	0.02	0.02	0.02	0.02	0.03	0.02
MgO	0.19	0.61	0.15	0.10	0.49	0.40	1.05	0.09	0.14	0.09
CaO	1.88	2.07	1.55	1.30	1.68	1.26	1.61	0.74	0.61	0.69
Na_2O	3.32	3.24	2.86	2.72	2.73	2.63	2.41	3.84	3.91	2.90
K_2O	4.29	4.27	5.11	6.37	5.32	7.29	3.40	4.71	3.73	7.54
P_2O_5	0.03	0.13	0.02	0.03	0.08	0.24	0.07	0.13	0.18	0.07
Sum	98.51	98.65	98.65	98.26	98.63	98.35	98.26	98.16	99.94	100.31
(ppm)										
V	8	21	5	12	16	16	39	9	7	10
Cr	5	6	5	5	10	3	23	3	39	2
Co	4	3	<LD	<LD	4	4	10	4	8	4
Ni	44	51	10	9	17	10	35	6	1	<LD
Zn	15	35	12	11	29	25	54	15	17	6
Ga	14	16	16	14	13	16	13	20	23	13
As	4	1	4	<LD	1	3	<LD	2.00	<LD	<LD
Rb	123.2	166.7	160.4	196.1	194.2	184.6	124.3	234.6	211.0	208.0
Sr	274.4	274.1	304.0	296.2	285.7	383.3	227.1	55.6	14.2	328.3
Y	11.1	16.3	3.1	5.3	8.6	19.3	5.6	12.2	8.2	6.4
Zr	23.8	19.3	6.4	37.7	24.7	39.5	90.2	14.7	18.4	8.9
Nb	3.3	12.6	2.9	1.4	9.1	5.5	15.1	14.8	36.9	1.0
Cs	1.1	3.4	1.9	2.0	2.9	2.2	2.3	5.0	2.7	1.1
Ba	957	935	1203	1162	1328	2147	884	107	23	1483
La	12.4	51.9	4.8	12.5	34.9	9.9	11.4	3.2	3.5	4.2
Ce	23.6	91.2	9.3	24.2	62.7	21.3	22.1	5.9	7.3	7.6
Pr	2.8	11.1	1.1	2.8	7.4	2.7	2.6	0.7	0.8	0.8
Nd	9.3	34.6	3.5	8.9	22.9	10.0	8.3	2.0	2.9	2.8
Sm	2.12	5.98	0.63	1.69	3.87	2.52	1.51	0.75	0.89	0.59
Eu	0.96	1.30	1.12	1.05	1.34	2.18	1.16	0.37	0.04	0.50
Gd	2.12	4.85	0.52	1.48	2.94	2.93	1.43	1.05	0.87	0.53
Tb	0.37	0.69	0.09	0.22	0.43	0.58	0.24	0.28	0.20	0.11
Dy	1.96	3.16	0.46	1.00	1.81	3.42	1.12	1.78	1.39	0.88
Ho	0.42	0.61	0.11	0.19	0.32	0.72	0.20	0.39	0.26	0.23
Er	1.04	1.38	0.29	0.46	0.67	1.68	0.43	1.19	0.81	0.91
Tm	0.16	0.20	0.05	0.07	0.09	0.24	0.06	0.23	0.15	0.17
Yb	0.89	1.13	0.33	0.49	0.51	1.21	0.32	1.63	1.17	1.27
Lu	0.14	0.18	0.05	0.09	0.08	0.18	0.05	0.27	0.17	0.20
Hf	0.81	0.58	0.25	3.19	0.66	1.17	2.30	0.74	0.90	0.40
Ta	<LD	1.04	0.44	<LD	0.58	0.32	0.81	3.74	6.75	0.19
Pb	27	25	27	37	31	59	36	52	17	37
Th	6.30	22.86	3.64	9.01	15.54	2.12	4.05	1.73	1.52	1.91
U	1.87	4.31	3.87	2.18	2.52	1.39	1.75	6.55	4.89	1.39
Eu/Eu*	1.38	0.74	5.98	2.03	1.21	2.45	2.41	1.27	0.15	2.74

	Leucosome			Basement orthogneiss		Basement paragneiss			
	AH-03-22	Mean	SEM[a]	AH-02-07	AH-02-12	AH-03-18	AH-02-28	AH-02-30	AH-03-21
(wt.%)									
SiO_2	74.49	73.34	1.27	67.91	70.15	71.36	58.21	68.32	57.54
TiO_2	0.07	0.14	0.11	0.53	0.34	0.17	2.01	0.16	2.04
Al_2O_3	14.41	14.01	0.50	14.77	14.59	16.33	15.19	17.16	13.63
Fe_2O_3*	0.48	0.55	0.25	1.82	1.18	0.73	3.00	0.68	3.28
FeO	0.56	0.71	0.40	2.67	1.52	0.88	5.51	0.90	5.99
MnO	0.03	0.02	0.01	0.07	0.04	0.03	0.13	0.03	0.13
MgO	0.12	0.35	0.25	1.15	0.74	0.46	2.58	0.62	2.83
CaO	0.74	1.46	0.52	3.06	2.31	2.11	4.76	2.96	4.75

Table 2 (*continued*)

	Leucosome			Basement orthogneiss		Basement paragneiss			
	AH-03-22	Mean	SEM[a]	AH-02-07	AH-02-12	AH-03-18	AH-02-28	AH-02-30	AH-03-21
Na_2O	3.80	3.27	0.52	3.96	3.42	4.45	2.20	5.23	2.11
K_2O	4.40	4.77	1.20	2.60	4.12	3.72	2.98	2.21	3.13
P_2O_5	0.15	0.09	0.06	0.15	0.11	0.07	0.86	0.10	0.97
Sum	99.25			98.69	98.52	100.32	97.44	98.36	96.40
(ppm)									
V	11	15	7	44	32	10	109	18	117
Cr	5	11	9	12	7	6	25	5	130
Co	3	5	2	8	5	7	19	3	23
Ni	<LD	22	19	27	52	<LD	36	31	87
Zn	16	22	10	69	45	29	148	35	143
Ga	17	16	2	22	16	19	15	18	23
As	<LD	2	1	3	4	<LD	2	4	<LD
Rb	221.0	174.4	35.2	155.1	181.9	117.8	168.9	79.3	140.7
Sr	18.5	231.9	94.2	255.6	295.6	426.7	557.0	617.0	454.7
Y	14.4	9.8	3.9	32.2	16.2	6.9	25.7	5.7	32.1
Zr	33.2	35.8	21.1	47.1	79.5	36.9	65.9	38.0	78.2
Nb	13.5	10.5	6.9	23.5	11.2	8.5	41.4	5.4	33.8
Cs	5.8	2.7	1.0	4.8	4.1	1.3	5.0	1.5	3.9
Ba	16	877	489	441	854	909	1300	672	1129
La	6.5	14.7	10.6	60.4	62.2	13.6	103.0	6.3	65.0
Ce	13.8	27.3	18.5	102.8	110.8	27.1	249.0	12.0	202.0
Pr	1.6	3.2	2.2	12.5	13.5	2.9	25.0	1.4	27.0
Nd	5.7	10.5	6.9	39.3	41.8	10.3	99.7	4.8	87.0
Sm	1.57	2.09	1.20	6.71	6.92	2.01	14.82	1.04	16.30
Eu	0.11	0.92	0.46	1.34	1.35	0.45	3.82	0.52	2.96
Gd	1.46	1.89	1.01	6.24	5.07	1.66	10.62	1.02	11.41
Tb	0.33	0.32	0.14	1.05	0.71	0.25	1.38	0.18	1.42
Dy	2.32	1.73	0.69	5.60	3.09	1.36	5.51	0.98	6.99
Ho	0.47	0.35	0.14	1.22	0.60	0.25	1.00	0.19	1.23
Er	1.52	0.92	0.35	3.08	1.44	0.63	2.13	0.44	3.09
Tm	0.28	0.15	0.06	0.46	0.21	0.08	0.30	0.06	0.40
Yb	2.12	0.95	0.43	2.61	1.21	0.47	1.68	0.36	2.48
Lu	0.32	0.15	0.07	0.41	0.20	0.06	0.24	0.05	0.34
Hf	1.30	1.36	0.83	1.20	2.17	1.30	1.57	1.20	2.00
Ta	2.27	1.60	1.45	1.33	0.67	0.59	1.92	0.35	1.65
Pb	26	32	9	18	25	23	20	22	16
Th	2.68	7.14	5.39	23.66	30.18	5.72	18.70	0.73	15.30
U	6.76	3.52	1.63	10.93	4.00	1.05	3.07	0.68	2.11
Eu/Eu∗	0.22			0.63	0.70	0.75	0.93	1.54	0.66

Major element analyses by X-Ray Fluorescence. Fe_2O_3∗ and FeO recalculated from measured Fe_2O_3T (total) using the procedure of Le Maitre (1976). Oxides normalized to 100% (anhydrous). Totals of measured analysis are reported in "sum" column. Trace element analyses carried out by X-Ray Fluorescence and Inductively Coupled Plasma-Mass Spectrometry. LD=Limit of Detection. $Eu/Eu* = Eu_{(N)}/[(Sm_{(N)} \times Gd_{(N)})^{1/2}]$; normalized using values from Sun and McDonough (1989).

[a] SEM is the standard error of the mean.

the host basement gneiss and the leucosome samples likely reflect fractionation of elements and migration of the melt from the source resulting in a melt that is preferentially enriched in LFSE relative to the HFSE and REE during partial melting (Sawyer, 1998). Similar compositions for the host gneiss and in situ leucosome are not expected. Depending on degrees of partial melting, melt extraction, and the nature of melting process (i.e. equilibrium melting or other melting mode), the mass balance of leucosome and melanosome would not necessarily yield a protolith composition (Sawyer, 1998; Kriegsman, 2001).

4.2. Whole rock radiogenic isotope geochemistry

Rubidium–strontium and neodymium–samarium data for whole rock samples of selected LBG and leucosome are presented in Table 3. Analytical details

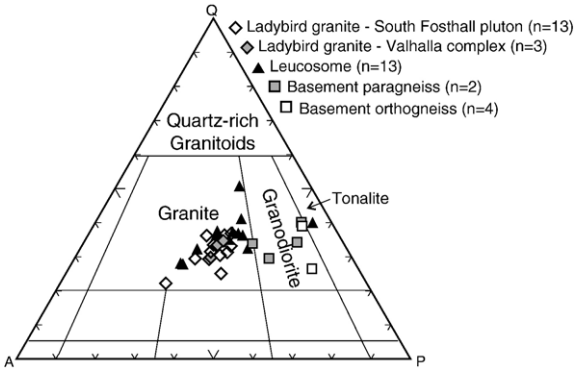

Fig. 4. Leucosome from Thor–Odin dome and leucogranite from the Ladybird granite suite plotted on Quartz–Alkali feldspar–Plagioclase (QAP) mesonormative-based classification scheme from Le Maitre (1989). All but one of the leucosome samples fall within the granite field.

are given in Appendix A.2. Ten leucosome and thirteen LBG whole rock samples were analyzed. In addition, four samples of basement gneiss were analyzed for the purposes of comparison, including two samples of basement paragneiss and two samples of basement orthogneiss (Table 3).

4.2.1. Sr isotopes

The LBG samples have highly variable radiogenic $^{87}Sr/^{86}Sr$ ratios that range from 0.70626 to 0.73812 with initial ratios ranging from 0.74256 to 0.73646 calculated at an age of 55 Ma, based on U–Pb zircon ages on the LBG suite (Carr, 1992). The $^{87}Rb/^{86}Sr$ ratios range from 0.29 to 7.35 (Fig. 9). The leucosome samples have higher measured $^{87}Sr/^{86}Sr$ ratios ranging from 0.74341 to 0.76718 with calculated initial ratios ranging from 0.74256 to 0.76593 at 55 Ma; details of the calculation are given in Table 3. The $^{87}Rb/^{86}Sr$ ratios of the leucosome define a tighter group than the LBG samples, with ratios that range from 0.56 to 1.98 (Fig. 9).

The four basement orthogneiss samples overlap with both the leucosome (basement samples AH-02-28 and AH-03-18) and the LBG samples (basement samples AH-02-07 and AH-02-12; Fig. 9). Basement samples have measured $^{87}Sr/^{86}Sr$ ratios ranging from 0.72418 to 0.75236 and $^{87}Rb/^{86}Sr$ ratios from 0.80 to 1.79 (Fig. 9). The Sr isotopic ratios demonstrate the highly radiogenic nature of the Paleoproterozoic basement gneisses in the Thor–Odin dome area.

At 55 Ma, the primitive mantle had an $^{87}Sr/^{86}Sr$ value of 0.70443, calculated assuming present day values of $^{87}Sr/^{86}Sr=0.7045$ and a bulk silicate earth $^{87}Rb/^{86}Sr$ of 0.089. The LBG samples display a wide range in radiogenic values, as do the leucosome samples; suggesting that both rock types were derived in large part from old, heterogeneous crustal material (Fig. 9). The differences in the range of Sr values observed between the leucosome and LBG samples are discussed below (see Section 5.2).

4.2.2. Nd isotopes

The LBG samples have a large range in $^{147}Sm/^{144}Nd$ ratios from 0.0996 to 0.15450 and $\varepsilon Nd_{(55\ Ma)}$ values from −5.0 to −17.2. The leucosome samples have a similar range with $^{147}Sm/^{144}Nd$ ratios from 0.1020–0.1521 and $\varepsilon Nd_{(55\ Ma)}$ values from −9.5 to −23.6 (Fig. 10). The four basement gneiss samples have $^{147}Sm/^{144}Nd$ ratios of 0.0895 to 0.1176 and $\varepsilon Nd_{(55\ Ma)}$ values of −19.8 to −27.0. The εNd was calculated at 55 Ma for direct comparison with the LBG and the leucosome samples, even though the basement gneiss samples are Paleoproterozoic in age (see Hinchey, 2005).

The range in $\varepsilon Nd_{(55\ Ma)}$ values observed in the LBG and the leucosome samples likely reflects heterogeneity in the source material. The strongly negative $\varepsilon Nd_{(55\ Ma)}$ of both the LBG and the leucosome samples indicates that the parental magmas of these rocks likely formed by partial melting of old continental crust. In addition, the data trend toward higher εNd numbers suggesting either a component of mixing, isotopic disequilibrium, and/or heterogeneity in their respective source materials.

4.2.3. Isotopic composition of potential sources

The majority of peraluminous muscovite-bearing granites are interpreted as being derived by partial melting of the crust, with exception given to rare, extreme

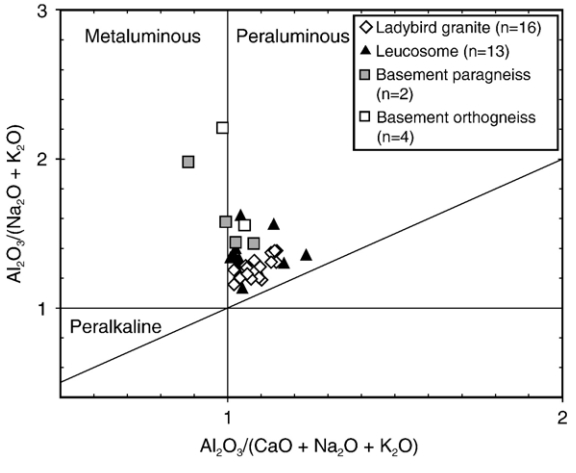

Fig. 5. Samples of Ladybird granite and leucosome plotted on Shand's plot of Al saturation index (molecular Al/(Ca+Na+K)) versus alkali saturation index (molecular Al/(Na+K)) from Maniar and Piccoli (1989). All samples fall within the peraluminous field.

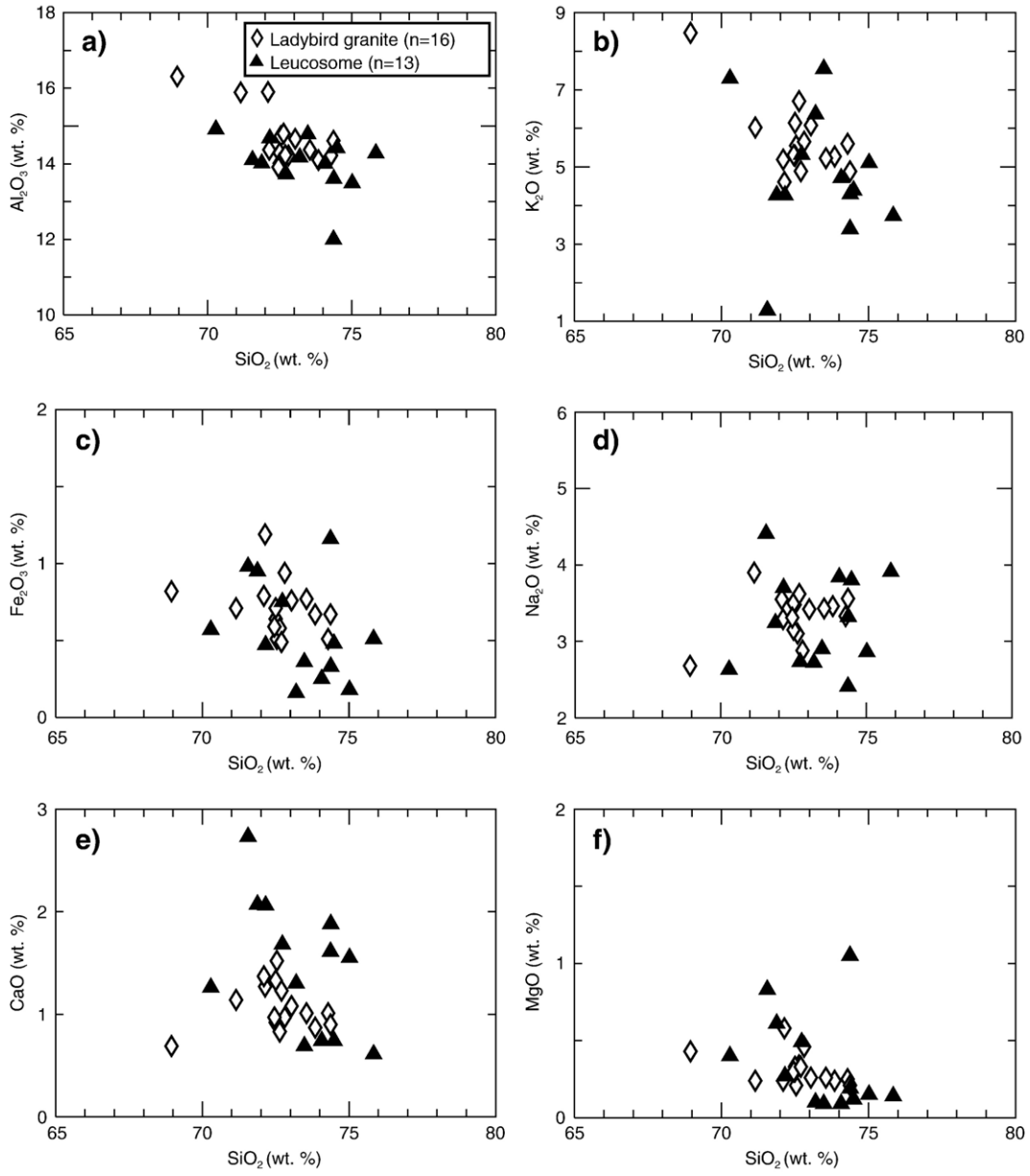

Fig. 6. SiO_2 versus major element (Harker) diagrams of the Ladybird granite and the leucosome samples, including (a) Al_2O_3, (b) K_2O, (c) Fe_2O_3, (d) Na_2O, (e) CaO, and (f) MgO. Values are listed in Table 2.

fractionation of I-type granitic magmas or local contamination (Barbarin, 1996; Sylvester, 1998). The LBG is a muscovite-bearing peraluminous leucogranite with high initial Sr ratios and is interpreted to have been derived by partial melting of the continental crust. This is supported by the $\varepsilon Nd_{(today)}$ and Sr ratios which are far too evolved to have formed via fractional crystallization of a mantle melt based on determined mantle values $\varepsilon Nd_{(today)}$ of $+6\pm1.5$ and $^{87}Sr/^{86}Sr$ of 0.7040 ± 0.0005. The mantle values beneath the Cordillera are based on data from mantle xenoliths, primitive Coast Belt granitoids, and primitive late Triassic to early Jurassic granitoids (Xue et al., 1990; Sun et al., 1991; Friedman et al., 1995; Ghosh, 1995). The most likely source material for the genesis of the LBG is the North American crust, which in this region can be essentially divided into two components the North American basement gneisses, composed of both ortho- and paragneiss, and the overlying Proterozoic supracrustal sedimentary rocks. The isotopic composition of each component is discussed below.

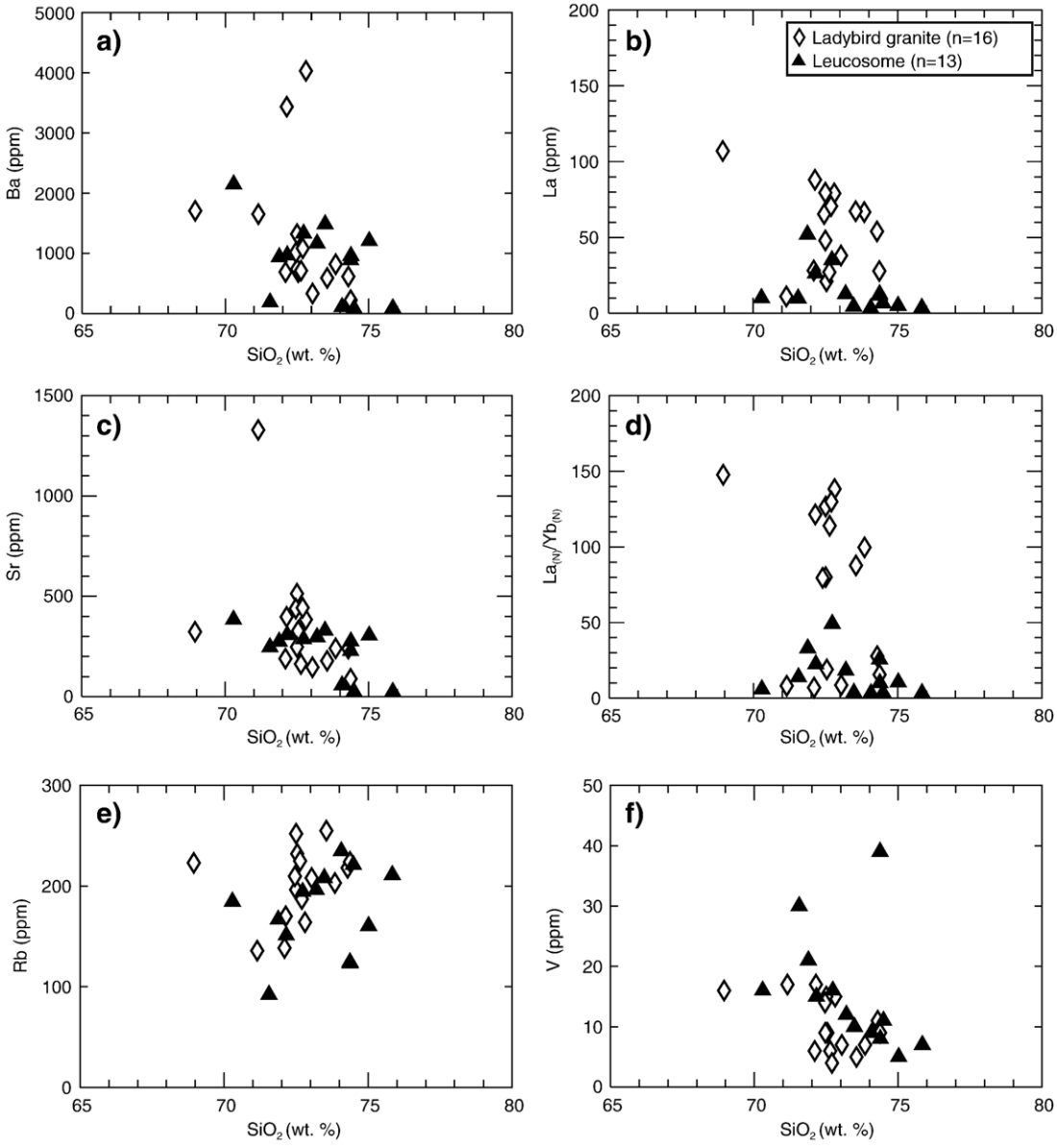

Fig. 7. SiO_2 versus selected trace elements or ratios of the Ladybird granite and the leucosome samples, including (a) Ba, (b) La, (c) Sr, (d) $La_{(N)}/Yb_{(N)}$, (e) Rb, and (f) V. Normalized values $_{(N)}$ are primitive mantle from Sun and McDonough (1989).

To assess the isotopic composition of the North American basement gneiss in the region, the data from this study is combined with data from basement gneisses from other localities in the Monashee complex. The upper part of the crystalline basement has a range in isotopic signatures. Armstrong et al. (1991) found that $^{87}Sr/^{86}Sr_{(measured)}$ ranges from 0.7114 to 2.179 and $\varepsilon Nd_{(today)}$ ranges from −6.2 to −29.4 for crystalline basement exposed in Frenchman Cap dome. Parkinson (1991) found variable isotopic signatures in basement ortho- and paragneiss from Thor–Odin dome with $^{87}Sr/^{86}Sr_{(measured)}$ from 0.76306 to 0.79493 and $\varepsilon Nd_{(today)}$ from −21.7 to −31.1. Basement samples from this study show an array of values with $^{87}Sr/^{86}Sr_{(measured)}$ of 0.72418 to 0.75236 and $\varepsilon Nd_{(today)}$ of −19.8 to −27.0. The basement gneisses of Frenchman Cap dome and Thor–Odin dome have variable isotopic compositions, and assigning an average composition is therefore not realistic, and the basement gneiss are treated as having a range of values shown on the figures (e.g. Fig. 11).

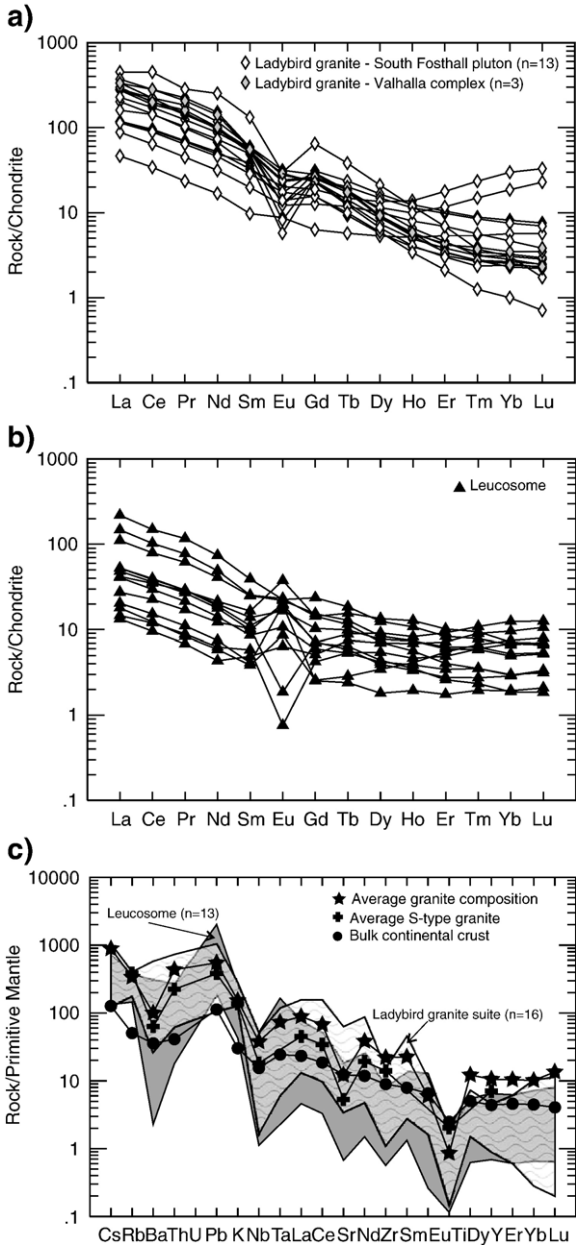

Fig. 8. Trace element normalized diagrams for the Ladybird leucogranite and leucosome samples. (a) Chondrite normalized diagram of the Ladybird leucogranite samples. (b) Chondrite normalized diagram of the leucosome samples. (c) Primitive mantle normalized diagram for the range of leucosome and the range of Ladybird leucogranite samples. Normalization from Sun and McDonough (1989). Bulk continental crust data from Taylor and McLennan (1995), average granite composition data from Govindaraju (1989), and average S-type granite data from Chappell and White (1992).

Several studies have constrained the isotopic signatures of the Proterozoic supracrustal rocks that were deposited on basement rocks. For the purpose of this paper, we evaluate the Windermere and Belt-Purcell Supergroups, which are the metasedimentary sequences most likely to overly basement rocks in the area. The isotopic composition of samples from the cover sequence of the Monashee complex is also evaluated as a potential source of melt. Samples of the cover sequence from Thor–Odin dome essentially overlap with basement samples and have a range of $^{87}Sr/^{86}Sr_{(measured)}$ from 0.7294 to 1.938 and $\varepsilon Nd_{(today)}$ from −6.7 to −25.1 (Parkinson, 1991). The isotopic signatures for the Windermere and Belt-Purcell Supergroups are plotted in Fig. 11.

5. Discussion

5.1. Petrogenesis of the Ladybird granite suite

The geochemical, isotopic and petrographic characteristics of the LBG samples support the formation of these leucogranites by the melting of a crustal source. The peraluminous nature of the leucogranites, in combination with the wide range of ages obtained from the inherited zircons (Carr, 1992), is typical of S-type granite and indicates that the crustal source was likely metasedimentary. The trace element composition of the LBG samples is compatible with granites that formed where garnet is stable in the crust, thus fractionating the HREE. This is supported by the enrichment of HREE in the two samples (AH-03-32 and AH-03-38) that contain xenocrysts of garnet. In addition, the negative Nb–Ta anomaly, negative Ti anomaly, and enrichment in incompatible elements (i.e. Sr, La, and Ba) are all consistent with magmas that formed via partial melting of the continental crust, although the negative Nb–Ta anomaly could also have been inherited from the source material. Considering all geochemical evidence, including major and trace element composition, isotopic composition, and peraluminous nature a pelitic-dominated source material is likely for the leucogranites.

The range in values, for both the Sr and Nd isotopes, indicate that the LBG plutons are isotopically heterogeneous. This can be explained by either a significant amount of crustal contamination or derivation from a source material that was isotopically heterogeneous. The magmas of the LBG likely formed by anatectic melting for the following reasons: a) leucogranites are not associated with mafic complements, which would be expected if the voluminous LBG formed via fractional crystallization from a more mafic magma; b) continental crust in this area was ~60–80 km thick prior to extension (Cook and Van der Velden, 1995; Clowes et

Table 3
Whole rock Sr and Nd isotope data of the leucosome, the Ladybird granite suite and basement gneiss samples from the Thor–Odin–Pinnacles area

Sr isotopes

Sample no.	Location	Rock type	Rb (ppm)	Sr (ppm)	$^{87}Sr/^{86}Sr$ (m)[a, b]	2σ [c] (+/−)	$^{87}Rb/^{86}Sr$ (calc)[d]	$^{87}Sr/^{86}Sr$ (55 Ma)
LB-02-01	Slocan Lake	Ladybird granite	196.3	513.0	0.713177	09	1.11	0.71231
LB-02-02	Slocan Lake	Ladybird granite	209.7	438.1	0.713340	10	1.39	0.71226
LB-02-03	Slocan Lake	Ladybird granite	187.1	442.7	0.712551	10	1.22	0.71160
AH-03-03	Slocan Lake	Ladybird granite	232.0	327.1	0.713635	12	2.05	0.71203
AH-03-06	Sugar Lake	Ladybird granite	203.0	240.1	0.716841	34	2.45	0.71493
AH-03-07	Sugar Lake	Ladybird granite	252.0	247.2	0.719191	21	2.95	0.71688
AH-03-13	Sugar Lake	Ladybird granite	224.0	88.3	0.724540	18	7.35	0.71880
AH-03-30	Mt. Baldur	Ladybird granite	223.0	322.9	0.733146	23	2.00	0.73158
AH-03-31	Mt. Baldur	Ladybird granite	170.0	397.1	0.714386	17	1.24	0.71342
AH-03-32	Mt. Baldur	Ladybird granite	138.4	189.2	0.738118	33	2.12	0.73646
AH-03-33	Mt. Baldur	Ladybird granite	164.0	383.8	0.716813	22	1.24	0.71585
AH-03-34	Mt. Baldur	Ladybird granite	225.0	162.3	0.736805	25	4.02	0.73366
AH-03-37	Mt. Baldur	Ladybird granite	135.8	1329.0	0.706258	17	0.30	0.70603
AH-02-05	Frigg Glacier	Leucosome	92.1	245.9	0.743413	14	1.09	0.74256
AH-02-06	Frigg Glacier	Leucosome	150.9	307.0	0.750247	15	1.43	0.74913
AH-02-08	Frigg Glacier	Leucosome	123.2	274.4	0.747273	19	1.30	0.74625
AH-02-09	Frigg Glacier	Leucosome	166.7	274.1	0.751479	12	1.77	0.75010
AH-02-10	Frigg Glacier	Leucosome	160.4	304.0	0.750216	11	1.53	0.74902
AH-02-11	Frigg Glacier	Leucosome	196.1	296.2	0.761240	11	1.92	0.75974
AH-02-13	Frigg Glacier	Leucosome	194.2	285.7	0.752558	17	1.98	0.75101
AH-02-26	Saturday Glacier	Leucosome	184.6	383.3	0.761799	65	1.40	0.76070
AH-02-27	Saturday Glacier	Leucosome	124.3	227.1	0.767178	11	1.59	0.76593
AH-03-20	Saturday Glacier	Leucosome	36.5	191.2	0.765469	16	0.56	0.76504
AH-02-07	Frigg Glacier	Orthogneiss	155.1	255.6	0.752361	16	1.76	0.75098
AH-02-12	Frigg Glacier	Orthogneiss	181.9	295.6	0.750427	24	1.79	0.74903
AH-02-28	Saturday Glacier	Paragneiss	168.9	557.0	0.724180	10	0.88	0.72349
AH-03-18	Saturday Glacier	Paragneiss	117.8	426.7	0.726997	24	0.80	0.72637

Nd isotopes

Sample no.	Location	Rock type	Sm (ppm)	Nd (ppm)	$^{143}Nd/^{144}Nd$ (m)[a, b]	2σ [c](+/−)	$^{147}Sm/^{144}Nd$ (calc)[d]	$^{143}Nd/^{144}Nd$ (55 Ma)	εNd [e] (55 Ma)
LB-02-01	Slocan Lake	Ladybird granite	9.13	55.18	0.512062	15	0.09964	0.51203	−10.6
LB-02-02	Slocan Lake	Ladybird granite	7.81	44.72	0.512047	10	0.10517	0.51201	−10.9
LB-02-03	Slocan Lake	Ladybird granite	8.10	47.45	0.512040	14	0.10280	0.51200	−11.0
AH-03-03	Slocan Lake	Ladybird granite	3.03	14.72	0.511890	68	0.12396	0.51185	−14.1
AH-03-06	Sugar Lake	Ladybird granite	8.66	45.82	0.511727	57	0.11381	0.51169	−17.2
AH-03-07	Sugar Lake	Ladybird granite	5.40	31.54	0.511785	37	0.10310	0.51175	−16.0
AH-03-13	Sugar Lake	Ladybird granite	5.87	22.88	0.511768	24	0.15450	0.51171	−16.7
AH-03-30	Mt. Baldur	Ladybird granite	20.20	118.00	0.511980	13	0.10309	0.51194	−12.2
AH-03-31	Mt. Baldur	Ladybird granite	8.93	71.01	0.512340	18	0.07573	0.51231	−5.0
AH-03-32	Mt. Baldur	Ladybird granite	5.00	24.26	0.512007	30	0.12411	0.51196	−11.8
AH-03-33	Mt. Baldur	Ladybird granite	8.48	65.94	0.512218	15	0.07744	0.51219	−7.4
AH-03-34	Mt. Baldur	Ladybird granite	4.37	21.51	0.511875	13	0.12234	0.51183	−14.4
AH-03-37	Mt. Baldur	Ladybird granite	1.49	7.85	0.512069	49	0.11430	0.51203	−10.5
AH-02-05	Frigg Glacier	Leucosome	1.31	6.62	0.512123	29	0.11916	0.51208	−9.5
AH-02-06	Frigg Glacier	Leucosome	3.8	19	0.511749	23	0.12044	0.51171	−16.8
AH-02-08	Frigg Glacier	Leucosome	2.12	9.29	0.511704	25	0.13742	0.51165	−17.8
AH-02-09	Frigg Glacier	Leucosome	5.98	34.57	0.511513	18	0.10417	0.51148	−21.3
AH-02-10	Frigg Glacier	Leucosome	0.63	3.49	0.511697	20	0.10871	0.51166	−17.7
AH-02-11	Frigg Glacier	Leucosome	1.69	8.86	0.511700	16	0.11487	0.51166	−17.7
AH-02-13	Frigg Glacier	Leucosome	3.87	22.85	0.511510	28	0.10199	0.51147	−21.3
AH-02-26	Saturday Glacier	Leucosome	2.52	9.98	0.511533	22	0.15206	0.51148	−21.2
AH-02-27	Saturday Glacier	Leucosome	1.51	8.31	0.511395	44	0.10942	0.51136	−23.6

Table 3 (*continued*)

Nd isotopes									
Sample no.	Location	Rock type	Sm (ppm)	Nd (ppm)	$^{143}Nd/^{144}Nd$ (m) [a, b]	2σ [c] (+/−)	$^{147}Sm/^{144}Nd$ (calc) [d]	$^{143}Nd/^{144}Nd$ (55 Ma)	εNd [e] (55 Ma)
AH-03-20	Saturday Glacier	Leucosome	0.27	1.48	0.511406	15	0.10986	0.51137	−23.4
AH-02-07	Frigg Glacier	Orthogneiss	6.71	39.26	0.511479	16	0.10292	0.51144	−22.0
AH-02-12	Frigg Glacier	Orthogneiss	6.92	41.78	0.511359	19	0.09974	0.51132	−24.3
AH-02-28	Saturday Glacier	Paragneiss	14.82	99.71	0.51216	17	0.08950	0.51118	−27.0
AH-03-18	Saturday Glacier	Paragneiss	2.01	10.29	0.51594	62	0.11763	0.51155	−19.8

[a] Measurements by TIMS.
[b] Measured and corrected for mass fractionation.
[c] Errors refer to last one or two digits and are propogated to include reproducibility of standard analysis and run errors.
[d] Calculated using ppm concentrations from ICP-MS trace element analysis.
[e] Calculated using present day chondritic uniform reservoir with $^{143}Nd/^{144}Nd = 0.512638$ and $^{147}Sm/^{144}Nd = 0.1967$.

al., 1995) and the over-thickened crust would have reached *P–T* conditions high enough to initiate melting of the middle crust (Patino-Douce et al., 1990); c) the Middle Crustal Zone, which the LBG largely intruded, and the structurally deeper, Thor–Odin dome, are characterized by sillimanite–potassium feldspar-melt assemblages (Reesor and Moore, 1971; Carr, 1992) supporting partial melting; d) the isotopic signature suggests melting of old, isotopically evolved crust; and e) the presence of abundant Proterozoic inherited zircon cores from samples of the LBG, dated by U–Pb technique are consistent with the age of potential source rocks (Parrish et al., 1988; Carr, 1990; Vanderhaeghe et al., 1999).

The two likely sources for the LBG are the North American basement gneiss and/or the supracrustal rocks deposited on basement, including the Windermere and Belt-Purcell Supergroups, as well as the Monashee cover sequence. The extreme variation in Sr isotopic signature of the LBG samples, as well as the basement gneisses and the supracrustal rocks make it impossible to use this isotope system to distinguish between potential source materials for partial melting (Fig. 9).

The Nd isotopic signatures do not show the same extreme variation as the Sr isotopes; however, the isotopic compositions of most of the potential source materials overlap (Fig. 11). Comparing the Nd isotopic composition of the LBG with the basement gneiss of Thor–Odin and Frenchman Cap domes, the Nd systematics could be explained by partial melting of the basement gneiss. In addition, melting of the supracrustal rocks of Thor–Odin dome could also have produced the LBG, as they are isotopically indistinguishable from those of basement. However, the Windermere and Belt-Purcell supergroups do not display the same wide range in isotopic composition as the LBG, and this, coupled with the limited known extent of these units in the Thor–Odin area, supports the

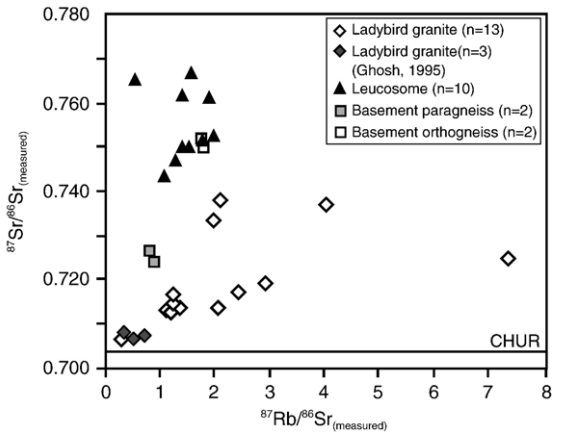

Fig. 9. $^{87}Rb/^{86}Sr_{(measured)}$ versus $^{87}Sr/^{86}Sr_{(measured)}$ diagram for samples of the Ladybird granite, the leucosome and selected basement gneiss for comparison. CHUR = chondritic uniform reservoir. See text for interpretation.

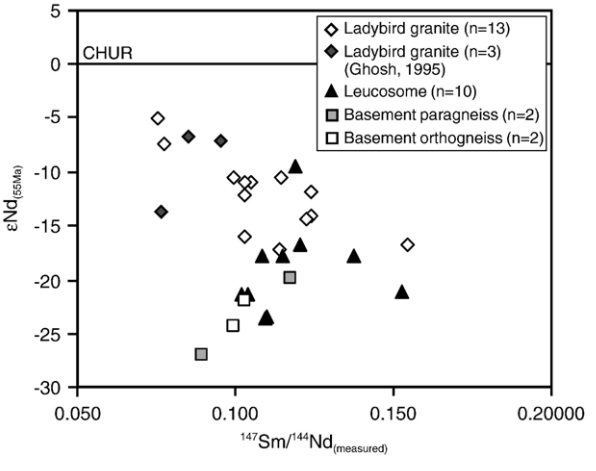

Fig. 10. $^{147}Sm/^{144}Nd_{(measured)}$ versus $\varepsilon Nd_{(55\ Ma)}$ diagram for samples of the Ladybird granite, the leucosome and selected basement gneisses for comparison. CHUR = chondritic uniform reservoir. See text for interpretation.

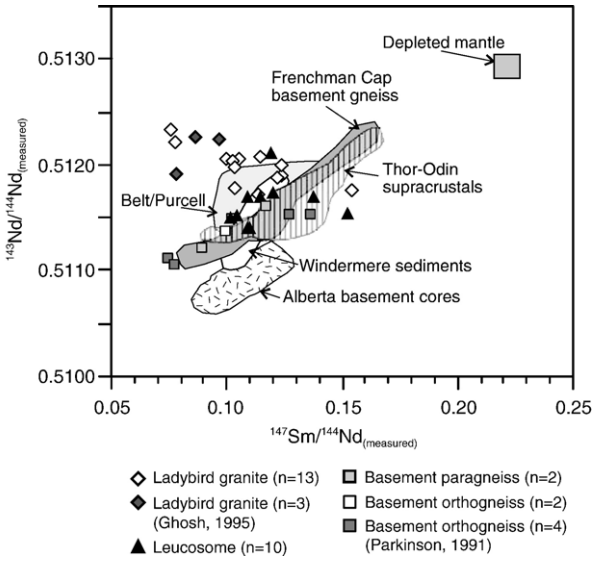

Fig. 11. $^{147}Sm/^{144}Nd_{(measured)}$ versus $^{143}Nd/^{144}Nd_{(measured)}$ diagram for samples of the Ladybird granite, the leucosome and selected basement gneisses from Thor–Odin dome. Basement orthogneiss from Thor–Odin dome (Parkinson, 1991; this study) are plotted for comparison. Fields for Thor–Odin dome supracrustals and Frenchman Cap dome basement gneisses are from Parkinson (1991) and Armstrong et al. (1991). Fields for Proterozoic Supergroups (Windermere, Belt-Purcell) and Archean basement cores for the Canadian Cordillera are also plotted for comparison. Data are from Frost and O'Nions (1984), Devlin et al. (1985), Frost and Burwash (1986), Frost and Winston (1987), Burwash et al. (1988), Devlin et al. (1988), Burwash and Wagner (1989), Ross et al. (1993) and Anderson and Goodfellow (2000). Depleted mantle values are from DePaolo (1988).

conclusion that melting of these metasedimentary rocks was not likely a major contributor to the formation of the South Fosthall pluton. However, regionally, it cannot be ruled out that melting of these supracrustal rocks may have contributed to the formation of parts of the suite.

5.2. Evidence for a genetic link between migmatites and leucogranites

Melting in the basement rocks was synchronous with emplacement of the Ladybird granites at higher structural levels (Carr, 1992; Vanderhaeghe et al., 1999; Hinchey et al., in press). This raises the question as to whether the migmatites preserved in the basement rocks of Thor–Odin dome may be the source for the Ladybird granites. In terms of major and trace element composition, significant differences observed between the LBG and the leucosome samples are: a) slightly lower LREE concentration in the leucosome samples; and, b) lower concentrations of most of the HFSE in the leucosome. Similar REE relationships in other leucosome studies have been attributed to disequilibrium melting (Barbero et al., 1995; Watt et al., 1996; Jung et al., 1999, 2000). Sawyer (1987) attributed leucosome with high abundances of HFSE and negative Eu anomalies to represent fractionated melts, and leucosome with lower REE concentrations and positive Eu anomalies to represent cumulates. The cumulate model was supported by Ellis and Obata (1992), who found that the anhydrous nature of leucosome and the lack of retrograde reactions suggested that the leucosome does not represent frozen melt segregation but rather cumulates that precipitated from the melt. Johannes et al. (2003) documented the same chemical patterns of low abundance of HFSE and positive Eu anomaly in leucosome samples while the associated granites had higher HFSE concentrations and negative Eu anomalies. They also attributed this chemical pattern to the leucosome representing cumulates and the granites representing the final melts. The difference in geochemical signature of the Thor–Odin dome leucosome and the Ladybird granites can be explained by a similar model, whereby the leucosome samples are the cumulates and the LBG suite the residual melts that formed during deformation assisted segregation of melt. There are two samples of vein leucosome that have the same chemical pattern as the leucogranites (AH-03-17 and AH-03-22). These samples crosscut all of the host rock types and foliation in the area, and based upon these relationships and their chemistry, are interpreted to represent residual melts.

The Nd isotopic data from the leucosome samples overlap with those of the LBG suite, although their Sr isotopic composition is clearly more radiogenic. This seemingly contradictory relationships can be explained in a number of ways: a) the isotopic heterogeneity may

reflect variation in the isotopic composition of the source material, which can result in a large range in isotopic composition of the anatectic melts. It has been demonstrated that Sr isotopic heterogeneity within source rocks may be preserved on the mineralogical scale before and during anatexis in some orogenic terranes (George and Bartlett, 1996), thus isotopic homogenization is not a necessary consequence of prograde metamorphism preceding anatexis (Knesel and Davidson, 2002). Variable Sr signatures have been documented in the Himalayan Manaslu peraluminous leucogranites, which show an extreme range in signatures on the meter scale (Deniel et al., 1987). This is characteristic of granites derived by low-melt fractions in short-lived systems typical of pure crustal melts (Barbero et al., 1995). A larger number of samples from the LBG may likely show significantly more isotopic heterogeneity and consequently show more overlap with leucosome samples. b) The LBG samples may have a more homogenous isotopic signature than the leucosome samples as they were mobilized from their source and emplaced into higher structural levels where they were mixed; a process which has been found to have homogenizing affects on isotopic signatures (Barbero et al., 1995). c) The differences in Sr isotopic signatures between the leucosome and LBG may be due to partial isotopic resetting during partial melting. Incomplete isotopic resetting during migmatite formation has been observed in areas of high-grade anatexis. Pelite-derived anatectic leucogranites have been documented with slightly higher initial εNd and lower initial $^{87}Sr/^{86}Sr$ than local leucosome, associated mesosome and granulite-facies pelitic material (Barbero et al., 1995). Isotopic disequilibrium is supported by experimental studies that show that the stoichiometry of melting reactions and the kinetics of melting are the major process controlling the isotopic composition of a melt, suggesting that isotopic composition is not controlled by the overall bulk composition of the source material (Hammouda et al., 1994). In a migmatite terrain, a relative enrichment of biotite and accessory minerals in the granites compared to the leucosome could explain isotopic differentiation and variability of Sr ratios. d) The Sr isotopic signature may be controlled by differences in melting reactions, which could control variations in the Sr isotopic composition of granite/leucosome melts from a single metapelitic source (Knesel and Davidson, 2002; Zeng et al., 2005). The experimental study of Knesel and Davidson (2002) showed that Ms-dehydration results in granites with higher $^{87}Sr/^{86}Sr_{(i)}$ and lower $Sr_{(ppm)}$ concentrations than the source rocks, whereas the fluid fluxed melting produced lower $^{87}Sr/^{86}Sr_{(i)}$ and higher $Sr_{(ppm)}$ concentrations than the source rocks. Rapid melt extraction, a function of the feedback between melting and deformation, would stop the isotopic exchange between melt and source before equilibration, thus explaining batch melts from a single source with variable Sr isotopic signatures. These various models could explain the potential for slightly different Sr isotopic systematics in the Ladybird granite and leucosome samples.

Both leucosome and leucogranite sample contain inherited Precambrian zircon cores. In leucosome samples from the Thor–Odin dome, Hinchey et al. (in press) documented zircon with cores that range in age from 2.6 to 1.8 Ga, with a dominant age population of ca. 1.86 Ga and a smaller age population of ca. 2.05 Ga, and interpreted the cores as detrital grains that were inherited from the host gneiss and incorporated into the leucosome providing the nucleation site for Paleogene magmatic zircon growth during anatexis. The ages of inherited cores overlap with those from a study of structurally deeper leucosome in the southern flank of Thor–Odin dome, which documented (Vanderhaeghe et al., 1999) concordant cores at 1.8, 2.0 and 2.2 Ga and ages ranging from 1.8 to 2.4 Ga and interpreted the cores are inherited detrital grains. In initial U–Pb studies of the LBG by TIMS (Thermal Ionization Mass Spectrometry) analysis, abundant altered cores within zircons were documented (Parrish et al., 1988; Carr, 1992). It was not possible, in these studies, to determine a precise age of inheritance, although the range of ages was likely between 1.5 to 2.5 Ga (Parrish et al., 1988; Carr, 1990). In an in situ (SHRIMP) zircon study of the LBG, Vanderhaeghe et al. (1999) documented highly discordant rims ranging from 1.0 to 2.2 Ga, with more concordant grains of ca. 1.8 Ga age. Discordant ages younger than 1.8 Ga are likely a result of mixing between inherited 1.8 Ga cores and the ca. 56 Ma zircon. The age of inherited zircon cores in the LBG and leucosome samples indicates that both lithologies were likely sourced by melting of paragneiss dominated by Paleoproterozoic detrital zircon.

Much of the geochemical and isotopic evidence presented here indicates a strong correlation between the leucosome and the Ladybird granite samples. These include major element concentrations, trace element concentrations, Nd isotopics, coeval U–Pb zircon ages, as well as the general restriction of the peraluminous leucogranites to amphibolite facies metamorphic zones and the abundant inherited Precambrian zircon in both lithologies. This evidence suggests that the melting in

the basement gneisses that produced the anatectic leucosome may have also produced portions of the LBG suite. The chemical signatures suggest that most of the leucosome represents cumulates and that the LBG are residual melts. The regional extent of the LBG and the difficulty in distinguishing, at least isotopically, between the different supracrustal sequences makes it impossible to rule out melting of the overlying supracrustal rocks as potential contributors to the formation of the Ladybird granites. However, the data presented in this paper strongly supports a genetic link between the melting of ca. 26 to 33 km deep North American basement gneisses and the emplacement of at least part of the peraluminous LBG.

6. Summary of conclusions

Based upon the geochemical, isotopic, and field data from the peraluminous Ladybird granites and the basement leucosome several conclusions can be drawn.

1) The ca. 55 Ma South Fosthall pluton is a peraluminous, S-type leucogranitic intrusion and is part of the ca. 62 to 52 Ma Ladybird granite suite.
2) Thor–Odin dome basement gneisses are an exposure of North American basement rocks exhumed from ca. 26 to 33 km depths and contain abundant anatectic leucosome (15–50%) that formed via partial melting of the host paragneiss from ca. 56 to possibly as young as 51 Ma.
3) The Thor–Odin dome leucosome and the Ladybird granite samples have similar major and trace element chemistry. They are classified in the peraluminous granitic fields on discrimination diagrams. Differences in HFSE concentrations and Eu anomalies suggest that the leucosome and leucogranites are related as cumulates and residual melts, respectively.
4) The initial Nd isotope values for the Ladybird granite suite overlap with those of the leucosome samples. Both suites of samples have a range in initial $\varepsilon Nd_{(55\ Ma)}$ values; −5.0 to −17.2 for the leucogranites and −9.5 to −23.6 for the leucosome samples. The similarity of initial isotopic ratios supports a genetic link between the two.
5) The initial Sr isotope values for both the peraluminous leucogranites and leucosome samples show a large range in values. The initial Sr isotope ratios for the LBG suite (0.70603 to 0.73688) are slightly lower than those of the leucosome samples (0.74256 to 0.76593). This isotopic heterogeneity suggests either: a) isotopic disequilibrium during partial melting in the mid- to lower crust where the leucosome formed; b) the distribution of Sr during partial melting was controlled by different melt reactions; and/or, c) isotopic heterogeneity in the source rocks.
6) At least part of the LBG suite likely formed via partial melting of North American basement rocks. The abundant leucosome in the exhumed basement rocks of Thor–Odin dome, in addition to the geochemical, isotopic, and U–Pb data support this conclusion. The preservation of leucosome marks the melt migration paths for the overlying Ladybird granites. The platformal supracrustal metasedimentary rocks that overly basement may have also contributed regionally to the formation of parts of the suite.

Acknowledgements

This contribution is part of the Ph.D. dissertation of AMH at Carleton University. Financing for this study was provided by a Natural Sciences and Engineering Research Council grant to SDC and scholarships to AMH were provided by Carleton University and an Ontario Graduate Scholarship. Helpful comments by Tony Fowler and Tracy Rushmer and critical reviews by C. Villaseca and an unknown reviewer greatly improved the clarity of the manuscript. We thank many people at Carleton University for assistance, including B. Cousens and J. Blenkinsop for help with Sm–Nd and Rb–Sr analyses.

Appendix A. Analytical methods

A.1. Whole rock major and trace element geochemistry

Major elements and some trace elements (Cr, Ni, Cu, Zn, Ga, Y, Zr, Nb, Ba) were analyzed by X-Ray Fluorescence (XRF) on fused disks using a Philips PW 2400X-ray fluorescence spectrometer at the University of Ottawa. XRF precision is based on six replicate runs and was 0.71% for SiO_2, 0.27% for Al_2O_3, 0.74% for K_2O, 6.4% for Zn. The accuracy was monitored using international references DR-N and SY-2 and was within 0.6% for SiO_2, 0.3% for Al_2O_3, 0.8% for K_2O, 1.6% for Zn, and better than 1% and 10% for other major and trace elements, respectively. The REE and other trace elements were analyzed at Geoscience Laboratories in Sudbury, Ontario and at ACME analytical laboratories in Vancouver, British Columbia by Inductively Coupled Plasma Mass Spectrometry (ICP-MS) using a HP 4500 plus quadrupole instrument following a HNO_3–

$HClO_4$–HF–HCl digestion. This acid digestion technique was selected because of lower detection limits for many elements and the large number of elements analyzed. The precision of the REE analyses is based on seven replicates and was mostly better than 10%, but samples with concentrations close to detection limits had precision of only 20%. The accuracy of REE analyses was monitored by international references SY-4, BIR-1 and GSR-2, was better than 10% for materials with high concentrations of REE. As some trace element rich accessory phases are resistant to acid digestion, several samples were analyzed in duplicates using more rigorous combination of fusion and acid digestion. A comparison of 6 samples had precision for the REE mostly better than 10%, and therefore concerns about the effects of incomplete acid digestion are minimal.

A.2. Whole rock isotope geochemistry analytical methods

Rubidium–strontium and samarium–neodymium isotopic analyses were carried at the Carleton University. Powdered samples were each dissolved with 1 mL of doubly distilled HNO_3 and HF for 2 to 7 days. The samples were loaded onto columns with Dowex 50WX8 resin for Sr and initial REE-group separation. The Sm–Nd isotopic concentration and isotope dilution fractions were pipetted into Teflon columns using 2× 0.15N HCl to separate these elements from the rest of the REE. The Nd was removed for using 2× 0.17N HCl.

The Sr and Sm–Nd fractions were loaded separately on outgassed single Ta filaments and double Re filaments for analysis on a Finnegan MAT 261 thermal ionization mass spectrometer. The isotopic composition fractions were measured using the Faraday multi-collector routine, which collects 15 blocks of 10 scans, with on line drift and mass fractionation correction and statistical analysis. The $^{87}Sr/^{86}Sr$ and $^{143}Nd/^{144}Nd$ errors are reported to 2σ (95%) confidence intervals and were directly measured from the mass spectrometer. The $^{87}Rb/^{86}Sr$ and the $^{147}Sm/^{144}Nd$ ratio were calculated based on the measured Rb and Sr concentrations from the whole rock ICP-MS values. The estimated uncertainties, at the 2σ level, equate to a precision of 1% for the $^{147}Sm/^{144}Nd$ and $^{87}Sr/^{86}Sr$ ratios and the concentrations are reproducible to 0.5%. Based on numerous runs from September 1992 to October 2004 the La Jolla standard gave an average $^{143}Nd/^{144}Nd$ value of 0.511876 ± 0.00018 and the Sr standard NBS-987 gave an average $^{87}Sr/^{86}Sr$ value of 0.71025 ± 0.00003.

References

Anderson, H.E., Goodfellow, W.D., 2000. Geochemistry and isotope chemistry of the Moyie sills: implications for early tectonic setting of the Mesoproterozoic Purcell basin. In: Lydon, J.W., Höy, T., Slack, J.F., Knapp, M.E. (Eds.), The Geological Environment of the Sullivan Pb–Zn–Ag Deposit. Mineral Deposits Division of the Geological Association of Canada Special Publication, vol. 1, pp. 302–321.

Andronicos, C.L., Chardon, D.H., Hollister, L.S., Gehrels, G.E., Woodsworth, G.J., 2003. Strain partitioning in an obliquely convergent orogen, plutonism, and synorogenic collapse: Coast Mountains Batholith, British Columbia, Canada. Tectonics 22, 1–7.

Armstrong, R.L., 1988. Mesozoic and Early Cenozoic magmatic evolution of the Canadian Cordillera. Geological Society of America, Special Paper 218, 55–91.

Armstrong, R.L., Parrish, R.R., van der Hyden, P., Scott, K., Runkle, D., Brown, R.L., 1991. Early Proterozoic basement exposures in the southern Canadian Cordillera: core gneiss of Frenchman Cap, Unit 1 of the Grandforks Gneiss and Vaseaux Formation. Canadian Journal of Earth Sciences 28, 1169–1201.

Ashworth, J.R., 1985. Migmatites. Blackie and Sons Limited. 302 pp.

Barbarin, B., 1996. Genesis of the two main types of peraluminous granitoids. Geology 24, 295–298.

Barbero, L., Villaseca, C., Rogers, G., Brown, P.E., 1995. Geochemical and isotopic disequilibrium in crustal melting; an insight from the anatectic granitoids from Toledo, Spain. Journal of Geophysical Research, B, Solid Earth and Planets 100, 15,745–15,765.

Barbey, P., Brouand, M., Le-Fort, P., Pecher, A., 1996. Granite–migmatite genetic link: the example of the Manaslu Granite and Tibetan slab migmatites in central Nepal. Lithos 38, 63–79.

Brown, M., D'Lemos, R.S., 1991. The Cadomian granites of Mancellia, Northeast Armorican Massif of France; relationship to the St. Malo migmatite belt, petrogenesis and tectonic setting. Precambrian Research 51, 393–427.

Brown, M., Averkin, Y.A., McLellan, E.L., Sawyer, E.W., 1995. Melt segregation in migmatites. Journal of Geophysical Research, B, Solid Earth and Planets 100, 15655–15679.

Burwash, R.A., Wagner, P.A., 1989. Sm/Nd geochronology of the Moyie Intrusions, Moyie Lake map area, British Columbia (82G/5). Geological Fieldwork 1988; a Summary of Field Activities and Current Research. British Columbia Ministry of Energy, Mines and Petroleum Resources, Paper 1989-1, pp. 45–48.

Burwash, R.A., Cavell, P.A., Burwash, E.J., 1988. Source terranes for Proterozoic sedimentary rocks in southern British Columbia; Nd isotopic and petrographic evidence. Canadian Journal of Earth Sciences 25, 824–832.

Carr, S.D., 1990. Late Cretaceous–Early Tertiary tectonic evolution of the southern Omineca Belt, Canadian Cordillera. Ph. D. Thesis, Carleton University. 223 pp.

Carr, S.D., 1992. Tectonic setting and U–Pb geochronology of the Early Tertiary Ladybird Leucogranite suite, Thor–Odin–Pinnacles area, southern Omineca belt, British Columbia. Tectonics 11, 258–278.

Carr, S.D., Parrish, R.R., Brown, R.L., 1987. Eocene structural development of the Valhalla Complex, southeastern British Columbia. Tectonics 6, 175–196.

Chappell, B.W., White, A.J.R., 1992. I- and S-type granites in the Lachlan Fold Belt. Transactions of the Royal Society of Edinburgh. Earth Sciences 86, 1–26.

Chappell, B.W., White, A.J.R., 2001. Two contrasting granite types; 25 years later. Australian Journal of Earth Sciences 48, 489–499.

Clemens, J.D., 1990. The granulite–granite connection. In: Vielzeuf, D., Vidal, P. (Eds.), Granulites and Crustal Evolution, vol. 311, pp. 25–36.

Clowes, R.M., Zelt, C.A., Armor, J.R., Ellis, R.M., 1995. Lithospheric structure in the southern Canadian Cordillera from a network of seismic refraction lines. Canadian Journal of Earth Sciences 32, 1485–1513.

Cook, F.A., Van der Velden, A.J., 1995. Three-dimensional crustal structure of the Purcell Anticlinorium in the Cordillera of southwestern Canada. Geological Society of America Bulletin 107, 642–664.

Deniel, C., Vidal, P., Fernandez, A., Le Fort, P., Peucat, J.J., 1987. Isotopic study of the Manaslu granite (Himalaya, Nepal); inference on the age and source of Himalayan leucogranites. Contributions to Mineralogy and Petrology 96, 78–92.

DePaolo, D.J., 1988. Neodymium Isotope Chemistry: an Introduction. Springer-Verlag. 187 pp.

Devlin, W.J., Bond, G.C., Brueckner, H.K., 1985. An assessment of the age and tectonic setting of volcanics near the base of the Windermere Supergroup in northeastern Washington; implications for latest Proterozoic–earliest Cambrian continental separation. Canadian Journal of Earth Sciences 22, 829–837.

Devlin, W.J., Brueckner, H.K., Bond, G.C., 1988. New isotopic data and a preliminary age for volcanics near the base of the Windermere Supergroup, northeastern Washington, U.S.A. Canadian Journal of Earth Sciences 25, 1906–1911.

Duncan, I.J., 1984. Structural evolution of the Thor–Odin gneiss dome. Tectonophysics 101, 87–130.

Ellis, D.J., Obata, M., 1992. Migmatite and melt segregation at Cooma, New South Wales. Transactions of the Royal Society of Edinburgh. Earth Sciences 83, 95–106.

Friedman, R.M., Mahoney, J.B., Cui, Y., 1995. Magmatic evolution of the southern Coast Belt; constraints from Nd–Sr isotopic systematics and geochronology of the Southern Coast Plutonic Complex. Canadian Journal of Earth Sciences 32, 1681–1698.

Frost, C.D., Burwash, R.A., 1986. Nd evidence for extensive Archean basement in the western Churchill Province, Canada. Canadian Journal of Earth Sciences 23, 1433–1437.

Frost, C.D., O'Nions, R.K., 1984. Nd evidence for Proterozoic crustal development in the Belt-Purcell Supergroup. Nature (London) 312, 53–56.

Frost, C.D., Winston, D., 1987. Nd isotope systematics of coarse- and fine-grained sediments; examples from the Middle Proterozoic Belt-Purcell Supergroup. Journal of Geology 95, 309–327.

Gabrielse, H., Campbell, R.B., 1991. Upper Proterozoic assemblages, Chapter 6. In: Gabrielse, H., Yorath, C.J. (Eds.), Geology of the Cordilleran Orogen in Canada. Geology of Canada. Geological Survey of Canada, vol. 4, pp. 125–150.

George, M.T., Bartlett, J.M., 1996. Rejuvenation of Rb–Sr mica ages during shearing on the northwestern margin of the Nanga Parbat–Haramosh Massif. Tectonophysics 260, 167–185.

Ghosh, D.K., 1995. Nd–Sr isotopic constraints on the interactions of the Intermontane Superterrane with the western edge of North America in the southern Canadian Cordillera. Canadian Journal of Earth Sciences 32, 1740–1758.

Govindaraju, K., 1989. 1989 compilation of working values and sample description for 272 geostandards. Geostandards Newsletter 13, 1–113.

Hammouda, T., Pichavant, M., Chaussidon, M., 1994. Mechanisms of isotopic equilibration during partial melting; an experimental test of the behaviour of Sr. Mineralogical Magazine 58A, 368–369.

Hinchey, A.M., 2005. Thor–Odin dome: constraints on Paleocene–Eocene anatexis and deformation, leucogranite generation and the tectonic evolution of the southern Omineca belt, Canadian Cordillera. Ph.D. thesis, Carleton University. 236 pp.

Hinchey, A.M., Carr, S.D., 2003. Geochemical test for linkages in migmatitic basement rocks and the Ladybird granite suite; Thor–Odin dome, southeastern British Columbia. In: GAC-MAC 2003 Abstract Volume 28.

Hinchey, A.M., Carr, S.D., McNeill, P.D., Rayner, N., in press. Paleocene–Eocene high-grade metamorphism, anatexis and deformation in Thor–Odin dome, Monashee complex, southeastern British Columbia. Canadian Journal of Earth Sciences. Accepted 11/05.

Johannes, W., Ehlers, C., Kriegsman, L.M., Mengel, K., 2003. The link between migmatites and S-type granites in the Turku area, southern Finland. Lithos 68, 69–90.

Johnson, B.J., Brown, R.L., 1996. Crustal structure and Early Tertiary extensional tectonics on the Omineca belt at 51°N latitude, southern Canadian Cordillera. Canadian Journal of Earth Sciences 33, 1596–1611.

Jung, S., Hoernes, S., Masberg, P., Hoffer, E., 1999. The Petrogenesis of some migmatites and granites (Central Damara Orogen, Namibia): evidence for disequilibrium melting, wall-rock contamination and crystal fractionation. Journal of Petrology 40, 1241–1269.

Jung, S., Hoernes, S., Mezger, K., 2000. Geochronology and petrology of migmatites from the Proterozoic Damara Belt; importance of episodic fluid-present disequilibrium melting and consequences for granite petrology. Lithos 51, 153–179.

Kalsbeek, F., Jespen, H.F., Nutman, A.P., 2001. From source migmatites to plutons; tracking the origin of ca. 435 Ma S-type granites in the East Greenland Caledonian Orogen. Lithos 57, 1–21.

Knesel, K.M., Davidson, J.P., 2002. Insights into collisional magmatism from isotopic fingerprints of melting reactions. Science 296, 2206–2208.

Kretz, R., 1983. Symbols for rock-forming minerals. American Mineralogist 68, 77–279.

Kriegsman, L.M., 2001. Partial melting, partial melt extraction and partial back reaction in anatectic migmatites. Lithos 56, 75–96.

Kuiper, Y., 2003. Isotopic constraints on timing of deformation and metamorphism in the Thor–Odin dome, Monashee complex, southeastern British Columbia. Ph.D. Thesis. University of New Brunswick. 290 pp.

Le Breton, N., Thompson, A.B., 1988. Fluid-absent (dehydration) melting of biotite in metapelites in the early stages of crustal anatexis. Contributions to Mineralogy and Petrology 99, 226–237.

Le Maitre, R.W., 1976. Some problems of the projection of chemical data into mineralogical classifications. Contributions to Mineralogy and Petrology 56, 181–189.

Le Maitre, R.W. (Ed.), 1989. A Classification of Igneous Rocks and Glossary of Terms. Blackwell, Oxford. 193 pp.

Lonsdale, P.F., 1988. Paleogene history of the Kula Plate; offshore evidence and onshore implications. Geological Society of America Bulletin 100, 733–754.

Maniar, P.D., Piccoli, P.M., 1989. Tectonic discrimination of granitoids. Geological Society of America Bulletin 101, 635–643.

McNeill, P.D., Williams, P.F., 2003. Structural evolution of migmatites of the Thor–Odin area of the Monashee complex, southern British Columbia. In Cordilleran Tectonics Workshop 2003, Abstract Volume.

Mehnert, K.R., 1968. Migmatites and the Origin of Granitic Rocks. Elsevier Publishing Company. 405 pp.

Misch, P., 1968. Plagioclase compositions and non-anatectic origin of migmatitic gneisses in Northern Cascade Mountains of Washington State. Contributions to Mineralogy and Petrology 17, 1–70.

Monger, J.W.H., 1989. Overview of Cordilleran geology. In: Ricketts, B.D. (Ed.), Western Canada Sedimentary Basin; a Case History. Canadian Society of Petroleum Geologists, pp. 9–32.

Monger, J.W.H., Price, R.A., 2000. A transect of the southern Canadian Cordillera from Vancouver to Calgary. Geological Survey of Canada, Open File 3902. 170 pp.

Monger, J.W.H., Price, R.A., Tempelman-Kluit, D.J., 1982. Tectonic accretion and the origin of the two major metamorphic and plutonic welts in the Canadian Cordillera. Geology 10, 70–75.

Norlander, B.H., Whitney, D.L., Teyssier, C., Vanderhaeghe, O., 2002. Partial melting and decompression of the Thor–Odin Dome, Shuswap metamorphic core complex, Canadian Cordillera. Lithos 61, 103–125.

Obata, M., Yoshimura, Y., Nagakawa, K., Odawara, S., Osanai, Y., 1994. Crustal anatexis and melt migrations in the Higo metamorphic terrane, west-central Kyushu, Kumamoto, Japan. Lithos 32, 135–147.

Parkinson, D.L., 1991. Age and isotopic character of Early Proterozoic basement gneisses in the southern Monashee complex, southeastern British Columbia. Canadian Journal of Earth Sciences 28, 1159–1168.

Parkinson, D.L., 1992. Age and tectonic evolution of the southern Monashee complex, southeastern British Columbia; a window into the deep crust. PhD Thesis. University of California. 186 pp.

Parrish, R.R., Carr, S.D., Parkinson, D.L., 1988. Eocene extensional tectonics and geochronology of the southern Omineca Belt, British Columbia and Washington. Tectonics 7, 181–212.

Patino-Douce, A.E., Johnston, A.D., Humphreys, E.D., 1990. Closed system anatexis closed system anatexis in the Cordilleran interior; the importance of initial lithologic structure. Eos, Transactions American Geophysical Union 71, 298–299.

Pattison, D.R.M., Harte, B., 1988. Evolution of structurally contrasting anatectic migmatites in the 3-kbar Ballachulish aureole, Scotland. Journal of Metamorphic Geology 6, 475–494.

Price, R.A., 1986. The southeastern Canadian Cordillera: thrusting, tectonic wedging, and delamination of the lithosphere. Journal of Structural Geology 8, 239–254.

Reesor, J.E., Moore Jr., J.M., 1971. Petrology and structure of Thor–Odin gneiss dome, Shuswap metamorphic complex, British Columbia. Geological Survey of Canada, Paper, vol. 195. 149 pp.

Ross, G.M., Villeneuve, M.E., Parrish, R.R., Thériault, R.J., 1993. Tectonic assembly of crystalline basement, Alberta Basin; implications for mantle evolution and ancestry of Canada's Pacific margin. Lithoprobe Report, vol. 31, pp. 134–143.

Saunders, A.D., Tarney, J., Marsh, N.G., Wood, D.A., 1980. Ophiolites as ocean crust or marginal basin crust: a geochemical approach. In: Panayiotou, A. (Ed.), Ophiolites: Proceedings of the International ophiolite symposium, Nicosia, Cyprus 1979. Ministry of Agriculture and Natural Resources, Geological Survey Department, Cyprus, pp. 171–180.

Sawyer, E.W., 1987. The role of partial melting and fractional crystallization determining discordant migmatite leucosome compositions. Journal of Petrology 28, 445–473.

Sawyer, E.W., 1996. Melt segregation and magma flow in migmatites: implications for the generation of granite magmas. Transactions of the Royal Society of Edinburgh. Earth Sciences 87, 85–94.

Sawyer, E.W., 1998. Formation and evolution of granite magmas during crustal reworking: the significance of diatexites. Journal of Petrology 39, 1147–1167.

Sawyer, E.W., 2001. Melt segregation in the continental crust: distribution and movement of melts in anatectic rocks. Journal of Metamorphic Geology 19, 291–309.

Sevigny, J.H., Parrish, R.R., Ghent, E.D., 1989. Petrogenesis of peraluminous granites, Monashee Mountains, southeastern Canadian Cordillera. Journal of Petrology 30, 557–581.

Solar, G.S., Brown, M., 2001. Petrogenesis of migmatites in Maine, USA; possible source of peraluminous leucogranite in plutons? Journal of Petrology 42, 789–823.

Spark, R.N., 2001. Crustal thickening and tectonic denudation within the Thor–Odin culmination, Monashee complex, southern Canadian Cordillera. PhD Thesis, University of New Brunswick. 302 pp.

Struik, L.C., 1993. Intersecting intracontinental Tertiary transform fault systems in the North American Cordillera. Canadian Journal of Earth Sciences 30, 1262–1274.

Sun, S.-S., McDonough, W.F., 1989. Chemical and isotopic systematics of oceanic basalts: implications for mantle composition and processes. In: Saunders, A.D., Norry, M.J. (Eds.), Magmatism in Ocean Basins. Geological Society of London Special Publication, vol. 42, pp. 313–345.

Sun, M., Armstrong, R.L., Maxwell, R.J., 1991. Proterozoic mantle under Quesnellia; variably reset Rb–Sr mineral isochrons in ultramafic nodules carried up in Cenozoic volcanic vents of the southern Omineca Belt. Canadian Journal of Earth Sciences 28, 1239–1253.

Sylvester, P.J., 1998. Post-collisional strongly peraluminous granites. Lithos 45, 29–44.

Taylor, S.R., McLennan, S.M., 1995. The geochemical evolution of the continental crust. Reviews of Geophysics 33, 241–265.

Teyssier, C., Ferré, E., Whitney, D.L., Norlander, B., Vanderhaeghe, O., Parkinson, D., 2005. Flow of partially molten crust and origin of detachments during collapse of the Cordilleran orogen. In: Bruhn, D., Burlini, L. (Eds.), High-Strain Zones: Structures and Physical Properties. Geological Society of London Special Publication, vol. 245, pp. 39–64.

Vanderhaeghe, O., Teyssier, C., Wysoczanski, R., 1999. Structural and geochronological constraints on the role of partial melting during the formation of the Shuswap metamorphic core complex at the latitude of the Thor–Odin dome, British Columbia. Canadian Journal of Earth Sciences 36, 917–943.

Wanless, R.K., Reesor, J.E., 1975. Precambrian zircon age of orthogneiss in the Shuswap metamorphic complex, British Columbia. Canadian Journal of Earth Sciences 12, 326–332.

Watt, G.R., Burns, I.M., Graham, G.A., 1996. Chemical characteristics of migmatites: accessory phase distribution and evidence for fast melt segregation rates. Contributions to Mineralogy and Petrology 125, 100–111.

Wheeler, J.O., McFeely, P., 1991. Tectonic assemblage map of the Canadian Cordillera and adjacent parts of the United States of America: geological Survey of Canada, Map 17121, scale 1:2 000 000.

White, A.J.R., Chappell, B.W., 1990. Per migma ad magma downunder. Geological Journal 25, 221–225.

Xue, X., Baadsgaard, H., Irving, A.J., Scarfe, C.M., 1990. Geochemical and isotopic characteristics of lithospheric mantle beneath West Kettle River, British Columbia; evidence from ultramafic xenoliths. Journal of Geophysical Research, B 95, 15879–15891.

Zeng, L., Saleeby, J.B., Asimow, P., 2005. Nd isotope disequilibrium during crustal anatexis; a record from the Goat Ranch migmatite complex, southern Sierra Nevada Batholith, California. Geology 33, 53–56.